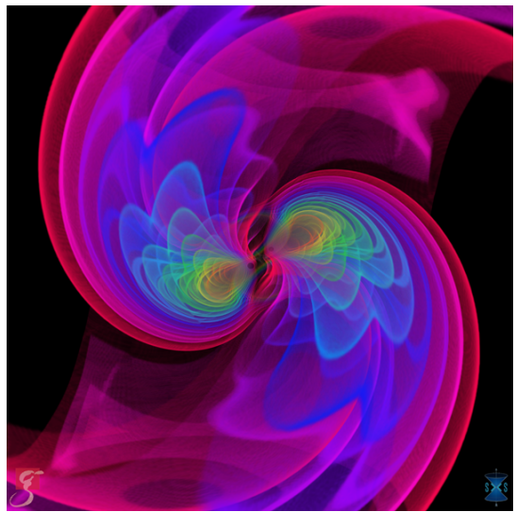

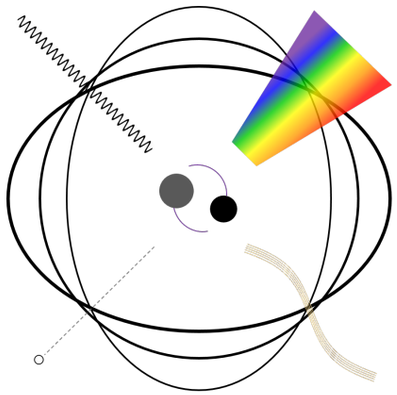
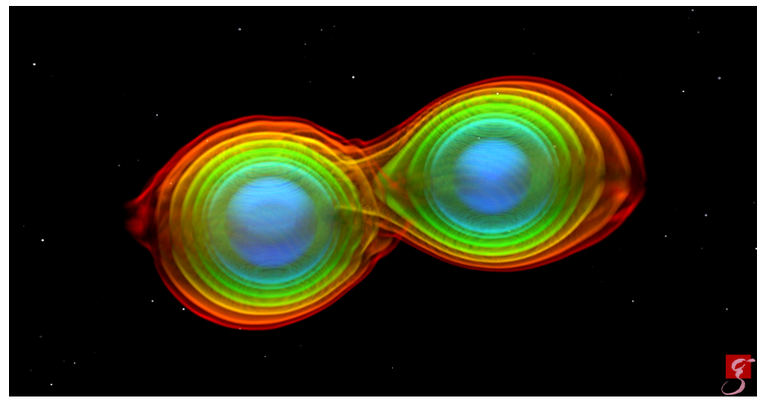

Effective-One-Body Theory, & Applications to Gravitational-Wave Observations

Alessandra Buonanno

Max Planck Institute for Gravitational Physics

(Albert Einstein Institute)

Department of Physics, University of Maryland

"Dublin School on Gravitational-Wave School Modeling", Dublin **June 11-12, 2018**

Outline

- **Lectures I-II:** Basics of gravitational waves

- **Lectures III-IV:** Motivations and development of effective-one-body (EOB) theory (two-body dynamics and waveforms)

- **Lecture V:** Using waveform models to infer astrophysical and cosmological information through gravitational-wave observations

- **Lecture VI:** Using waveform models to probe dynamical gravity and extreme matter with gravitational-wave observations

(NR simulation: Ossokine, AB & SXS @AEI)

(visualization credit: Benger @ Airborne Hydro Mapping Software & Haas @AEI)

References:

- **M. Maggiore's books**: "Gravitational Waves Volume 1: Theory and Experiments" (2007) & "Gravitational Waves Volume II: Astrophysics and Cosmology" (2018).

- **E. Poisson & C. Will's book**: "Gravity" (2015).

- **E.E. Flanagan & S.A. Hughes' review**: arXiv:0501041.

- **AB's Les Houches School Proceedings**: arXiv:0709.4682.

- **AB & B. Sathyaprakash's review**: arXiv:1410.7832.

- **UMD/AEI graduate course on GW Physics & Astrophysics** taught in Winter-Spring 2017: http://www.aei.mpg.de/2000472.

Parameters in GW from quasi-circular binary systems

Binary			GW propagation	Detector orientation
M, ν, S_1, S_2	$\theta_{S_1}, \theta_{S_2}, \phi_{S_1} - \phi_{S_2}$	~~$\theta_{\mathrm{L_N}}, \phi_{\mathrm{L_N}}$~~, $\phi_{S_1} + \phi_{S_2}$	Θ, φ	θ, ϕ, ψ
Basic	Local	Directional		

plus distance D & time at coalescence t_c

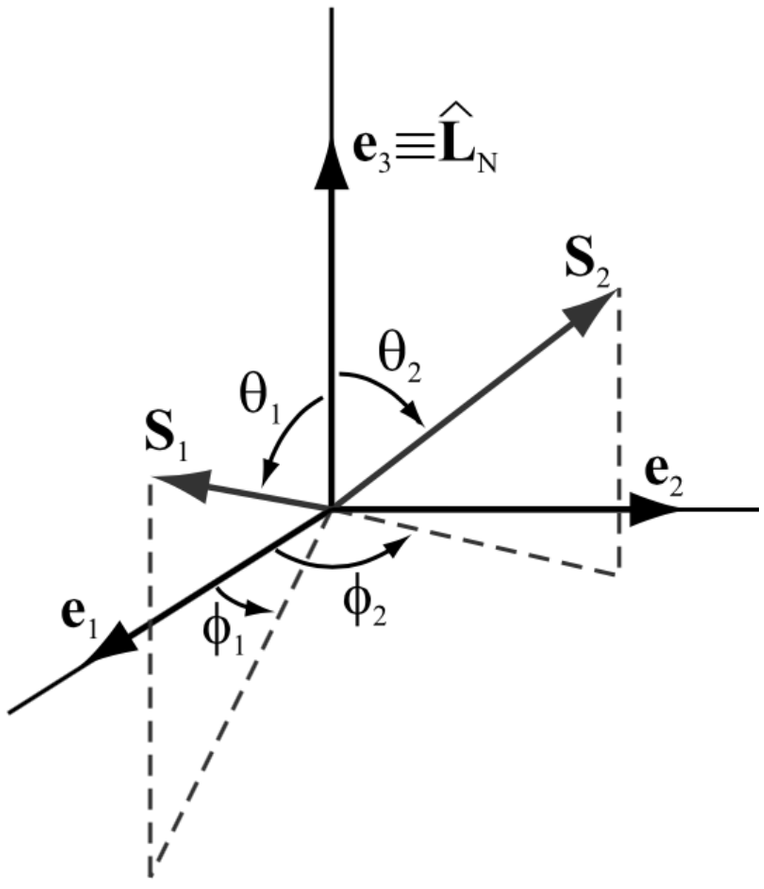

(AB, Chen & Vallisneri 03)

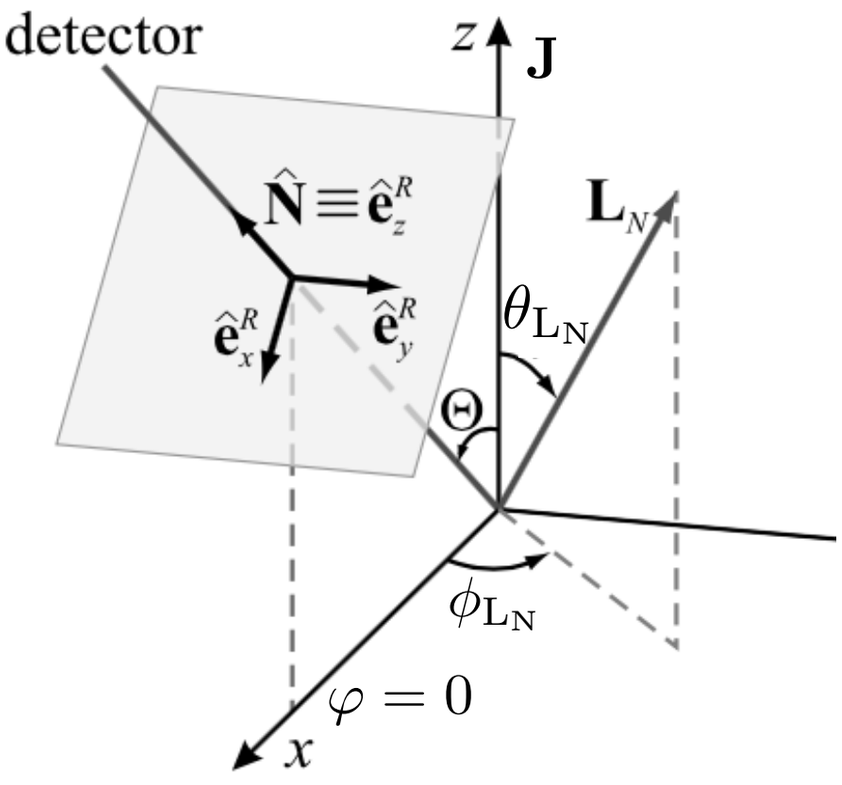

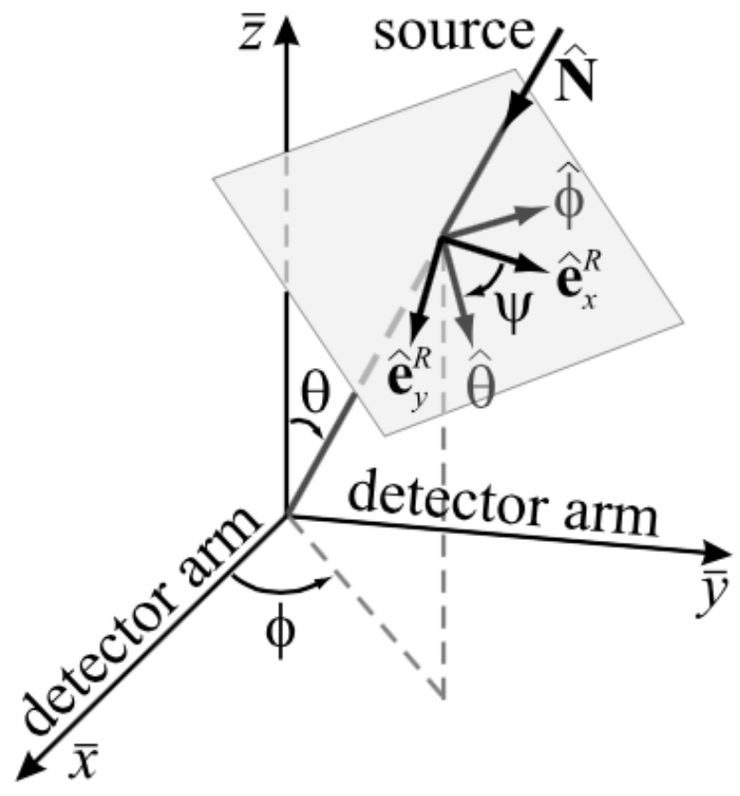

- **15 parameters** for waveforms from **quasi-circular** binary systems

GW polarizations in gravity

- **Generic metric theories of gravity** have **6** geometrically distinct **polarizations:**

(Will 72)

$$h_{ij}(\mathbf{x}) = \sum_A h_A(\mathbf{x})\, e^A_{ij} \qquad A = 1, \cdots, 6$$

6 amplitudes ↑ ↑ **6 polarization tensors**

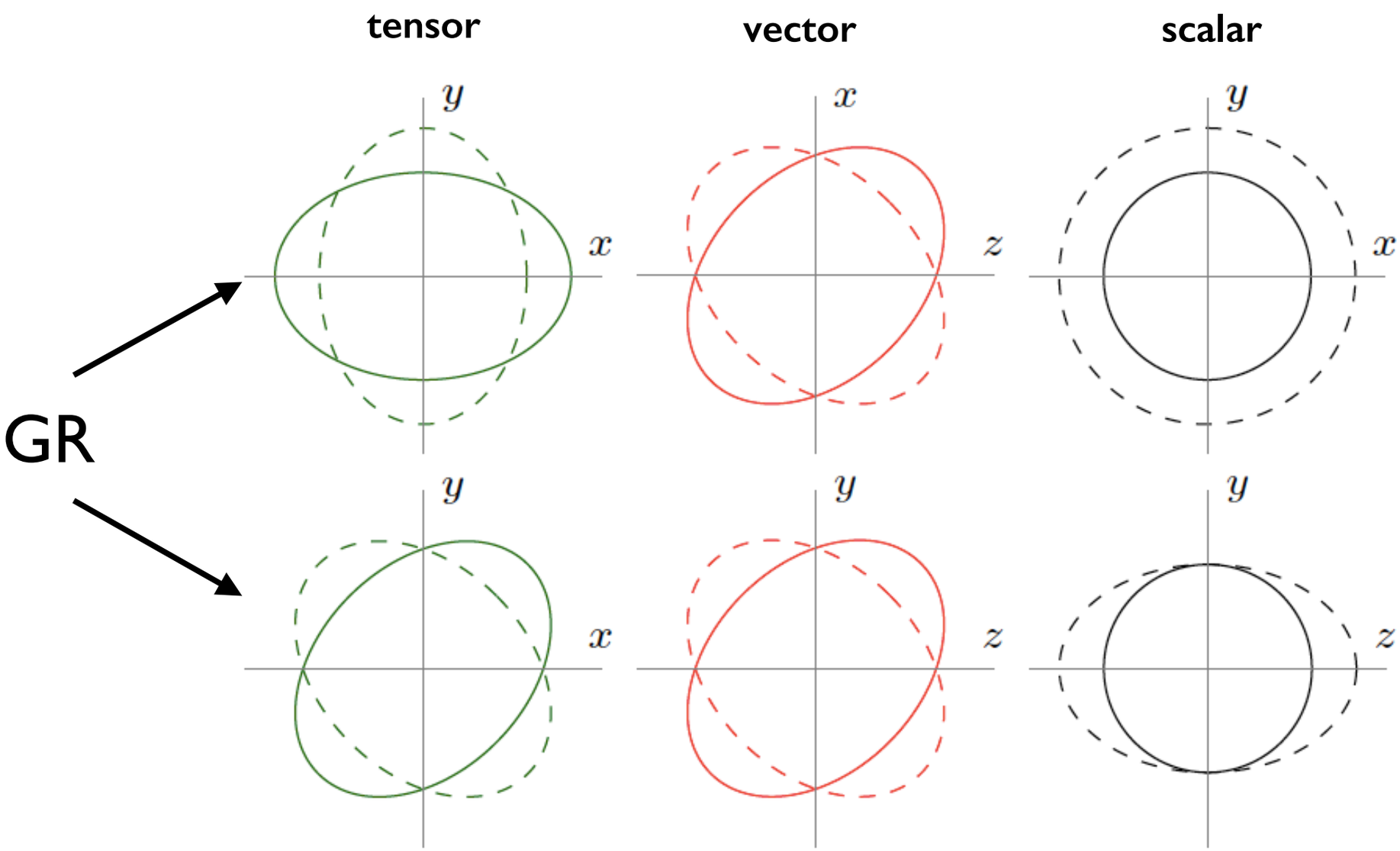

Detector antenna patterns for different GW polarizations

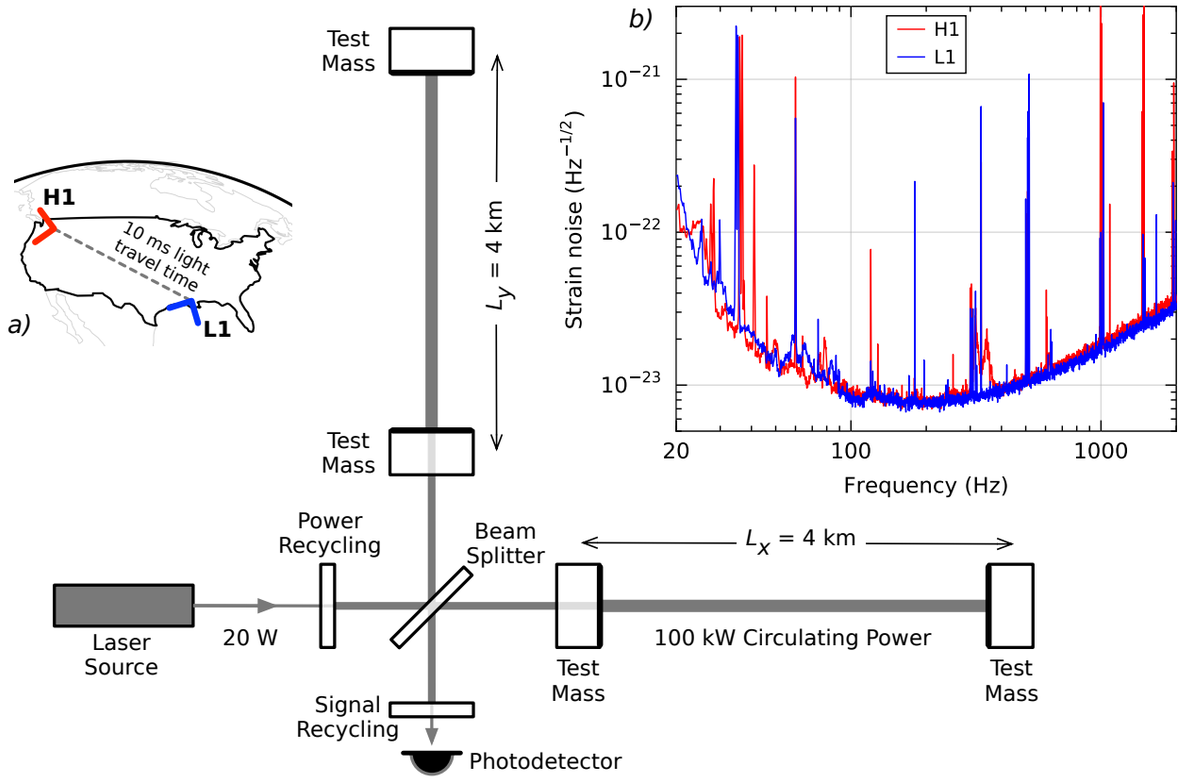

$$D^{ij} = \frac{1}{2}(d_x^i\, d_x^j - d_y^i\, d_y^j)$$ **differential-arm detector**

detector tensor

$$h_{\rm I}(t, \mathbf{x}_I) = D_I^{ij}\, h_{ij}(t, \mathbf{x}_I)$$

$$= \sum_A h_A(t, \mathbf{x}_I)\, (D_I^{ij}\, e_{ij}^A)$$

depends on GW source

depends only on geometry, F_A

- **Angular responses of a differential-arm detector**

$|F_A|$

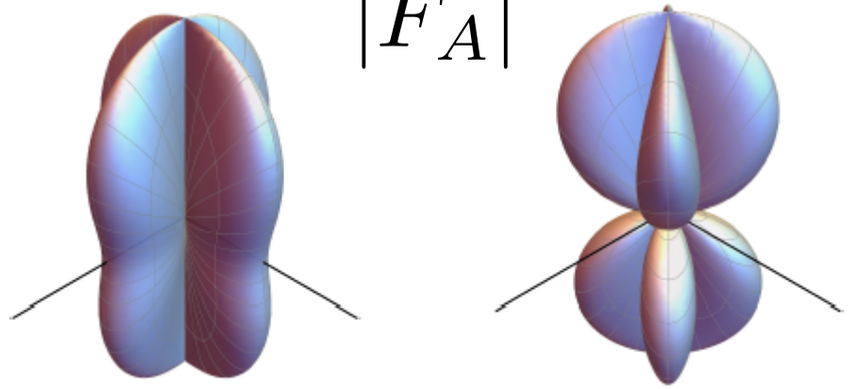

(a) Plus (+) (b) Cross (×)

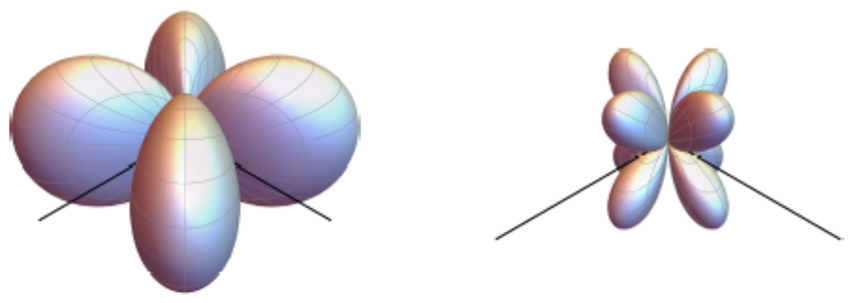

(c) Vector-x (x) (d) Vector-y (y)

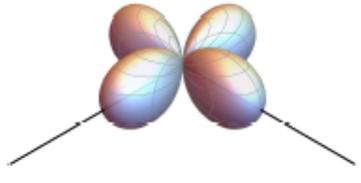

(e) Scalar (s)

Testing extra GW polarizations with two LIGOs & Virgo

detector tensor

$$h_{\rm I}(t,\mathbf{x}_I) = D_I^{ij}\, h_{ij}(t,\mathbf{x}_I)$$
$$= \sum_A h_A(t,\mathbf{x}_I)\,(D_I^{ij}\, e_{ij}^A)$$

depends on GW source

depends only on geometry, F_A

- **Angular responses of a differential-arm detector**

$|F_A|$

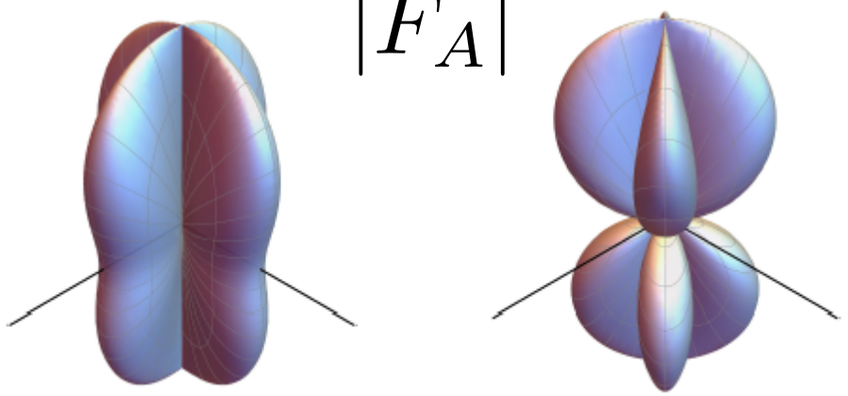

(a) Plus (+) (b) Cross (×)

examples of antenna patterns:

$$F_+(\vartheta,\varphi,\psi) = -\frac{1}{2}\left(1+\cos^2\vartheta\right)\cos 2\varphi\cos 2\psi$$

tensor

$$-\cos\vartheta\sin 2\varphi\sin 2\psi\ ,$$

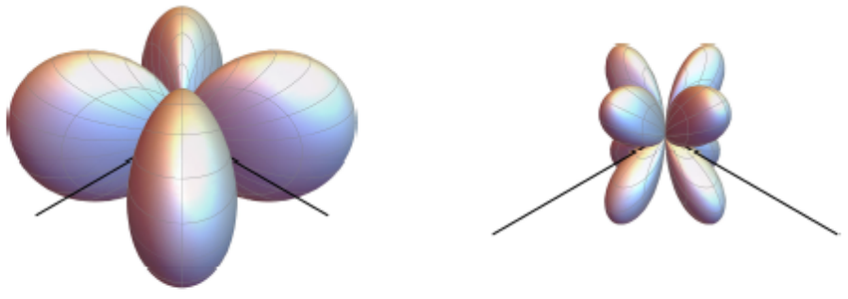

(c) Vector-x (x) (d) Vector-y (y)

$$F_{\rm b/l}(\vartheta,\varphi,\psi) = \mp\frac{1}{2}\sin^2\vartheta\cos 2\varphi$$

scalar

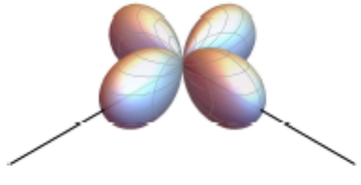

(e) Scalar (s)

- **Two LIGOs** are **nearly co-aligned,** approximately sensitive to the **same linear combination** of polarizations.

GW signal observed by ground-based detectors

- Polarizations for **non-spinning compact objects:**

$$h_+(t) = \frac{2\mathcal{M}}{D}\,(\mathcal{M}\omega)^{2/3}\,(1+\cos^2\Theta)\,\cos(2\Phi+2\Phi_0)$$

$$h_\times(t) = \frac{4\mathcal{M}}{D}\,(\mathcal{M}\omega)^{2/3}\,\cos\Theta\,\sin(2\Phi+2\Phi_0)$$ (Finn & Chernoff 93)

- Detector response: $h(t) = h_+(t)\,F_+ + h_\times(t)\,F_\times$

$$\widetilde{F}_\times = \frac{2\cos\Theta\,F_\times}{[(1+\cos^2\Theta)^2\,F_+^2+4\cos^2\Theta\,F_\times^2]^{1/2}} \qquad \widetilde{F}_+ = \frac{(1+\cos^2\Theta)\,F_+}{[(1+\cos^2\Theta)^2\,F_+^2+4\cos^2\Theta\,F_\times^2]^{1/2}}$$

$$\widetilde{F}_+^2 + \widetilde{F}_\times^2 = 1 \quad \Rightarrow \quad \cos\alpha \equiv \widetilde{F}_+ \quad \sin\alpha \equiv \widetilde{F}_\times$$

- Defining: $\mathcal{A}(\theta,\phi,\psi;\Theta) = [(1+\cos^2\Theta)^2\,F_+^2 + 4\cos^2\Theta\,F_\times^2]^{1/2}$

$$\tan\alpha(\theta,\phi,\psi;\Theta) = \frac{2\cos\Theta\,F_\times}{(1+\cos^2\Theta)\,F_+}$$

GW signal observed by ground-based detectors (contd.)

- Polarizations for **non-spinning compact objects:**

$$h_+(t) = \frac{2\mathcal{M}}{D}\,(\mathcal{M}\omega)^{2/3}\,(1+\cos^2\Theta)\,\cos(2\Phi+2\Phi_0)$$

$$h_\times(t) = \frac{4\mathcal{M}}{D}\,(\mathcal{M}\omega)^{2/3}\,\cos\Theta\,\sin(2\Phi+2\Phi_0)$$ (Finn & Chernoff 93)

- Detector response: $h(t) = h_+(t)\,F_+ + h_\times(t)\,F_\times$

$$h(t) = \frac{2\mathcal{M}}{D}\,\mathcal{A}\,[\mathcal{M}\omega(t)]^{2/3}\,\cos(2\Phi(t)+2\Phi_0-\alpha)$$

averaging over angles
$\overline{\mathcal{A}^2} = 16/25$

it can be re-absorbed in initial phase

- Defining:

$$\mathcal{A}(\theta,\phi,\psi;\Theta) = [(1+\cos^2\Theta)^2\,F_+^2 + 4\cos^2\Theta\,F_\times^2]^{1/2}$$

$$\tan\alpha(\theta,\phi,\psi;\Theta) = \frac{2\cos\Theta\,F_\times}{(1+\cos^2\Theta)\,F_+}$$

GW signal observed by ground-based detectors (contd.)

- Polarizations for **non-spinning compact objects:**

$$h_+(t) = \frac{2\mathcal{M}}{D}\,(\mathcal{M}\omega)^{2/3}\,(1+\cos^2\Theta)\,\cos(2\Phi+2\Phi_0)$$

$$h_\times(t) = \frac{4\mathcal{M}}{D}\,(\mathcal{M}\omega)^{2/3}\,\cos\Theta\,\sin(2\Phi+2\Phi_0)$$ (Finn & Chernoff 93)

- Detector response: $h(t) = h_+(t)\,F_+ + h_\times(t)\,F_\times$

$$h(t) = \frac{2\mathcal{M}}{D}\,\mathcal{A}\,[\mathcal{M}\omega(t)]^{2/3}\,\cos(2\Phi(t)+2\Phi_0-\alpha)$$

averaging over angles
$\overline{\mathcal{A}^2} = 16/25$

it can be re-absorbed in initial phase

- Fourier transform:

$$\tilde{h}(f) = \int_{-\infty}^{+\infty} e^{2\pi i f t}\,h(t)\,dt = \tfrac{1}{2}\int_{-\infty}^{+\infty} dt\,A(t)\,\left[e^{2\pi i f t + i\Phi_{\rm GW}(t)} + e^{2\pi i f t - i\Phi_{\rm GW}(t)}\right]$$

PN templates in stationary phase approximation

$$\tilde{h}(f) = \tfrac{1}{2} \int_{-\infty}^{+\infty} dt\, A(t)\, \left[e^{2\pi i f t + i\Phi_{\rm GW}(t)} + e^{2\pi i f t - i\Phi_{\rm GW}(t)} \right]$$

assuming $f > 0$

- **Dominant contribution from the vicinity of the *stationary* points in the phase**

(Sathyaprakash & Dhurandhar 91)

Assuming $f > 0$ and posing $\psi(t) \equiv 2\pi\, f\, t - \Phi_{\rm GW}$

Imposing $\left(\frac{d\psi}{dt}\right)_{t_f} = 0 \;\Rightarrow\; \left(\frac{d\Phi_{\rm GW}}{dt}\right)_{t_f} = 2\pi\, f = 2\pi F(t_f)$

Expanding the phase: $\psi(t_f) = 2\pi\, f\, t_f - \Phi_{\rm GW}(t_f) - \pi\, \dot{F}(t_f)\, (t - t_f)^2$

$$\tilde{h}_{\rm SPA}(f) = \frac{1}{2} \frac{A(t_f)}{\sqrt{\dot{F}(t_f)}}\, e^{i(2\pi\, f\, t_f - \Phi_{\rm GW}(t_f)) - i\pi/4}$$

- **How do we compute $\Phi_{\rm GW}(t_f)$ and $\dot{F}(t_f)$?**

PN templates in stationary phase approximation (contd.)

- **We need to solve** $v^3 = \dot{\Phi}_{\rm GW}\, M/2$ **and** $\dot{E}(v) = -F(v)$

$$t(v) = t_c + M \int_v^{v_c} dv\, \frac{E'(v)}{F(v)} \qquad E'(v) \equiv \frac{dE}{dv}$$

$$\Phi_{\rm GW}(v) = \Phi_c + 2 \int_v^{v_c} dv\, v^3\, \frac{E'(v)}{F(v)}$$ (Sathyaprakash & Dhurandhar 91)

$$\Rightarrow\ \psi(f) = 2\pi f\, t_c - \Phi_c - \pi/4 + 2\int_v^{v_c} (v_c^3 - v^3)\, \frac{E'(v)}{F(v)}\, dv$$

$$\Rightarrow\ \dot{F}(t_f) = \frac{\dot{\omega}}{\pi} = \frac{96}{5}\,\frac{1}{\pi}\,\nu\, M^{5/3}\, \omega^{11/3}$$

$$\tilde{h}_{\rm SPA}(f) = \mathcal{A}_{\rm SPA}(f)\, e^{i\psi_{\rm SPA}(f)} \qquad \mathcal{A}_{\rm SPA}(f) = \frac{\mathcal{A}}{r}\,\frac{1}{\pi^{2/3}}\,\left(\frac{5}{96}\right)^{1/2}\,\mathcal{M}^{5/6}\, f^{-7/6}$$

- $\psi_{\rm SPA}(f) = 2\pi\, f\, t_c - \Phi_c - \pi/4 + f^{-5/3}\,\left(\psi_0 + \psi_1\, f^{2/3} + \psi_{3/2}\, f + \cdots\right)$

$$\psi_0 = \psi_0(\mathcal{M})\,, \quad \psi_1 = \psi_1(m_1, m_2)\,, \quad \psi_{3/2} = \psi_{3/2}(m_1, m_2, \boldsymbol{S}\cdot\boldsymbol{L})\,, \cdots$$

GW amplitude in frequency domain during inspiral

(Abbott et al. PRX 6 (2016) 041015)

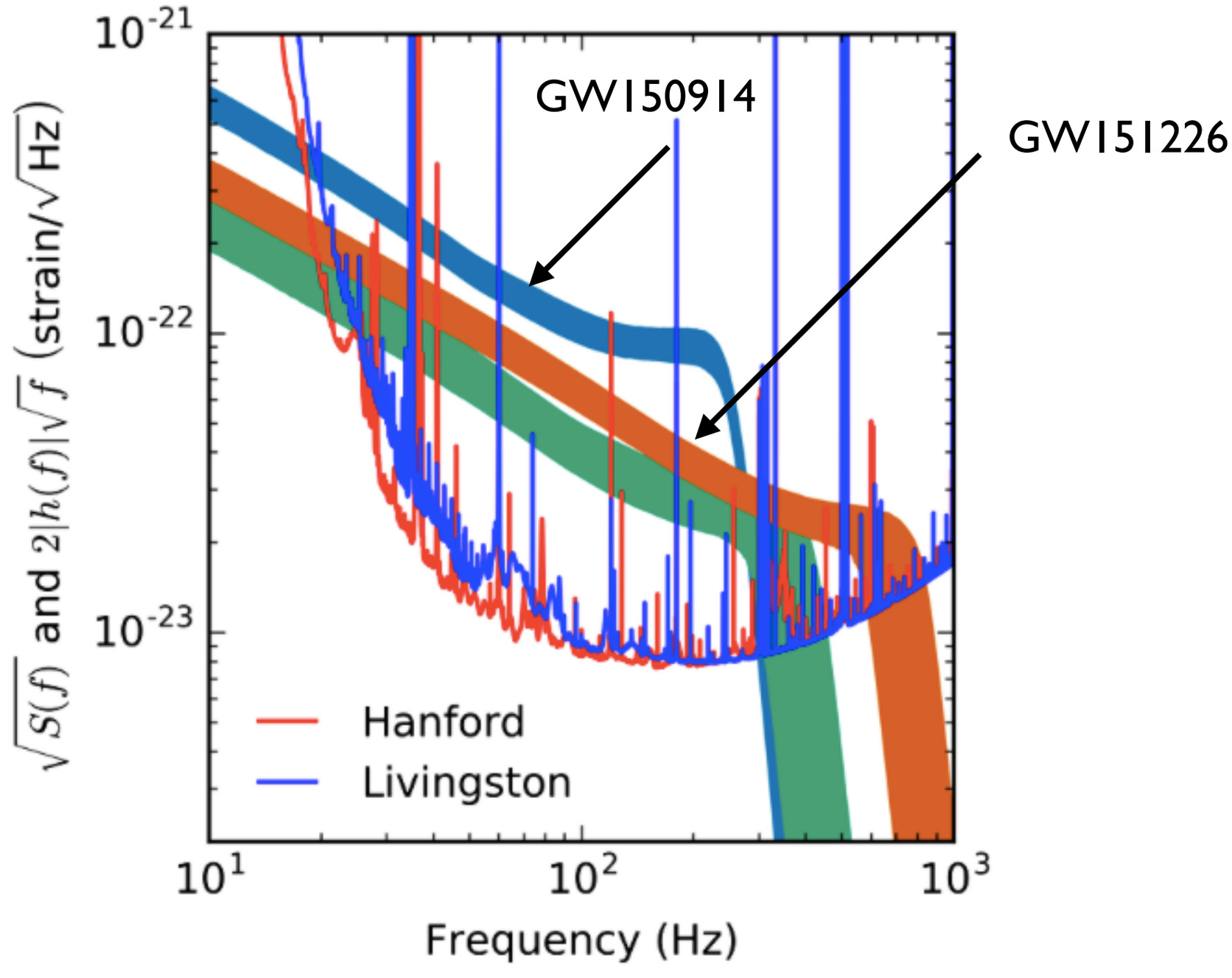

PN templates in stationary phase approximation: TaylorF2

$$\tilde{h}(f) = \mathcal{A}_{\rm SPA}(f)\, e^{i\psi_{\rm SPA}(f)}$$

$$\psi_{\rm SPA}(f) = 2\pi f t_c - \Phi_c - \pi/4 + \frac{3}{128}(\pi\mathcal{M}f)^{-5/3}\,\{1+$$

0PN

graviton with non zero mass

$$-\frac{5\hat{\alpha}^2}{336\omega_{\rm BD}}\nu^{2/5}\,(\pi\mathcal{M}f)^{-2/3} - \frac{128}{3}\frac{\pi^2 D\,\mathcal{M}}{\lambda_g^2(1+z)}\,(\pi\mathcal{M}f)^{2/3}$$

-1PN

1PN

dipole radiation

spin-orbit

$$+\left(\frac{3715}{756}+\frac{55}{9}\nu\right)\nu^{-2/5}\,(\pi\mathcal{M}f)^{2/3} - 16\pi\,\nu^{-3/5}\,(\pi\mathcal{M}f) + 4\beta\,\nu^{-3/5}\,(\pi\mathcal{M}f)$$

1PN

1.5PN

1.5PN

$$+\left(\frac{15293365}{508032}+\frac{27145}{504}\nu+\frac{3085}{72}\nu^2\right)\nu^{-4/5}\,(\pi\mathcal{M}f)^{4/3} - 10\sigma\,\nu^{-4/5}\,(\pi\mathcal{M}f)^{4/3}\Big\}$$

2PN

2PN

spin-spin

$$\beta = \frac{1}{12}\sum_{i=1}^{2}\chi_i\left[113\frac{m_i^2}{M^2}+75\nu\right]\widehat{\boldsymbol{L}}\cdot\widehat{\boldsymbol{S}}_i\,, \qquad \sigma = \frac{\nu}{48}\chi_1\chi_2\left(-27\widehat{\boldsymbol{S}}_1\cdot\widehat{\boldsymbol{S}}_2 + 721\widehat{\boldsymbol{L}}\cdot\widehat{\boldsymbol{S}}_1\widehat{\boldsymbol{L}}\cdot\widehat{\boldsymbol{S}}_2\right)$$

$$\chi_i = \frac{S_i}{m_i^2}$$

Waveforms encode plethora of physical effects

- Binary black hole

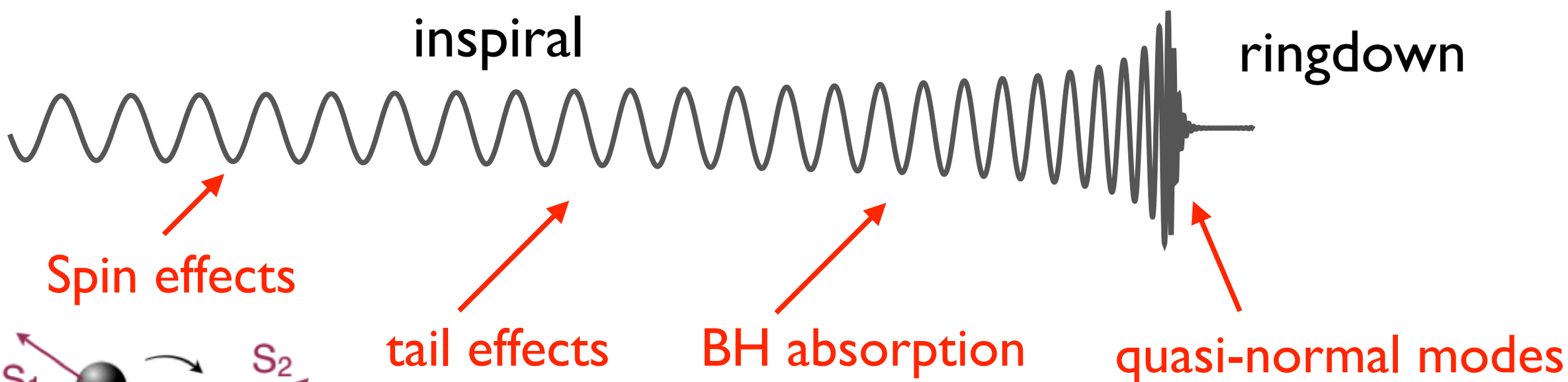

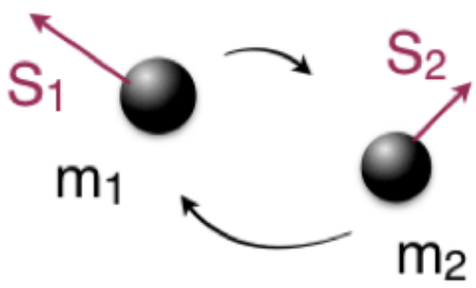

(credit: Hinderer)

- **Compact-object binary** with **matter** or in **modified theory** to GR?

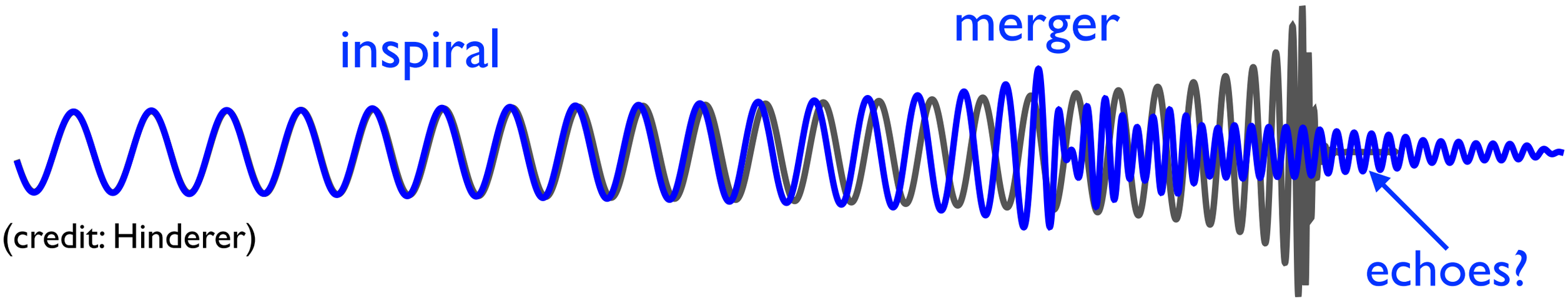

(credit: Hinderer)

Phenomenological waveforms used in O1 & O2 follow-up analyses

- First works in mid-late 2000 (Pan, AB et al. 07, Ajith et al. 07, Santamaria et al. 10)

- **Fast, frequency-domain** waveform model hybridizing and fitting EOB & NR (Khan et al. 15; Husa et al. 15; Hannam et al. 13)

$$\tilde{h}(f;\lambda_i) = \mathcal{A}(f;\lambda_i)\, e^{i\phi(f;\lambda_i)}$$

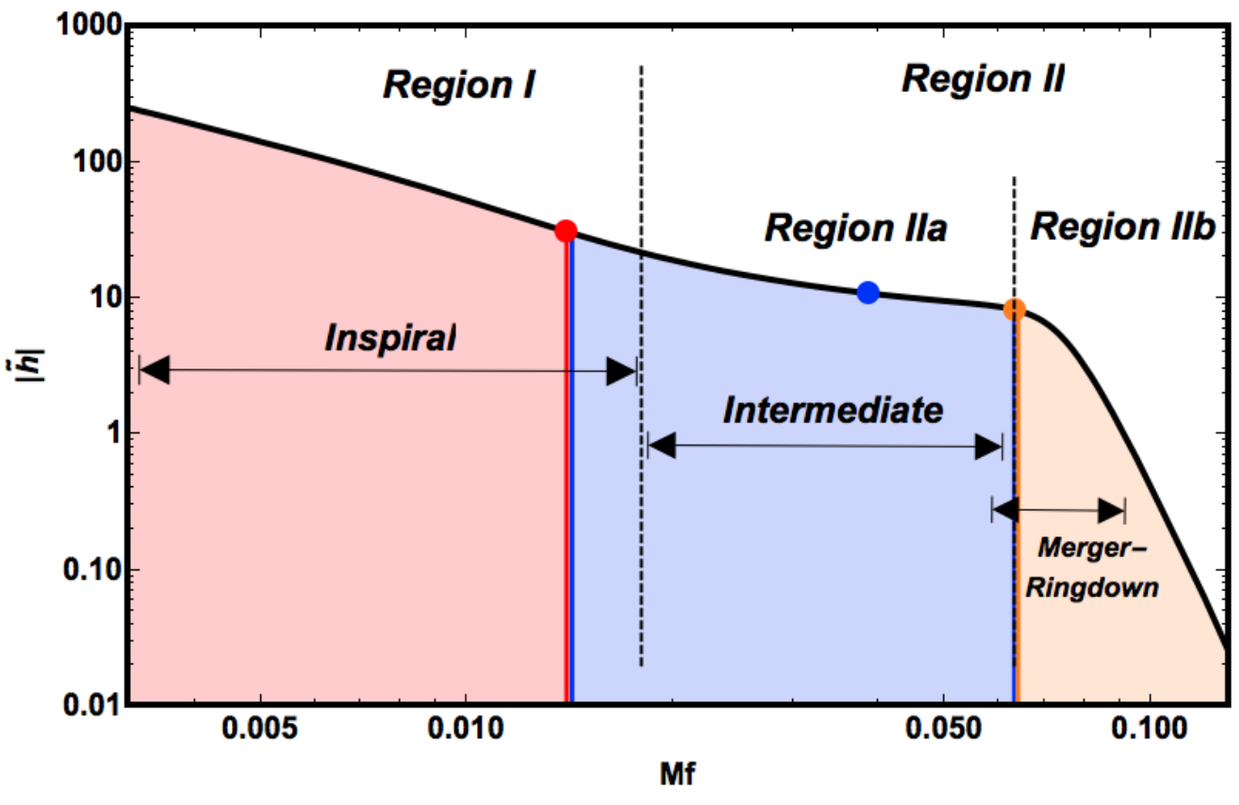

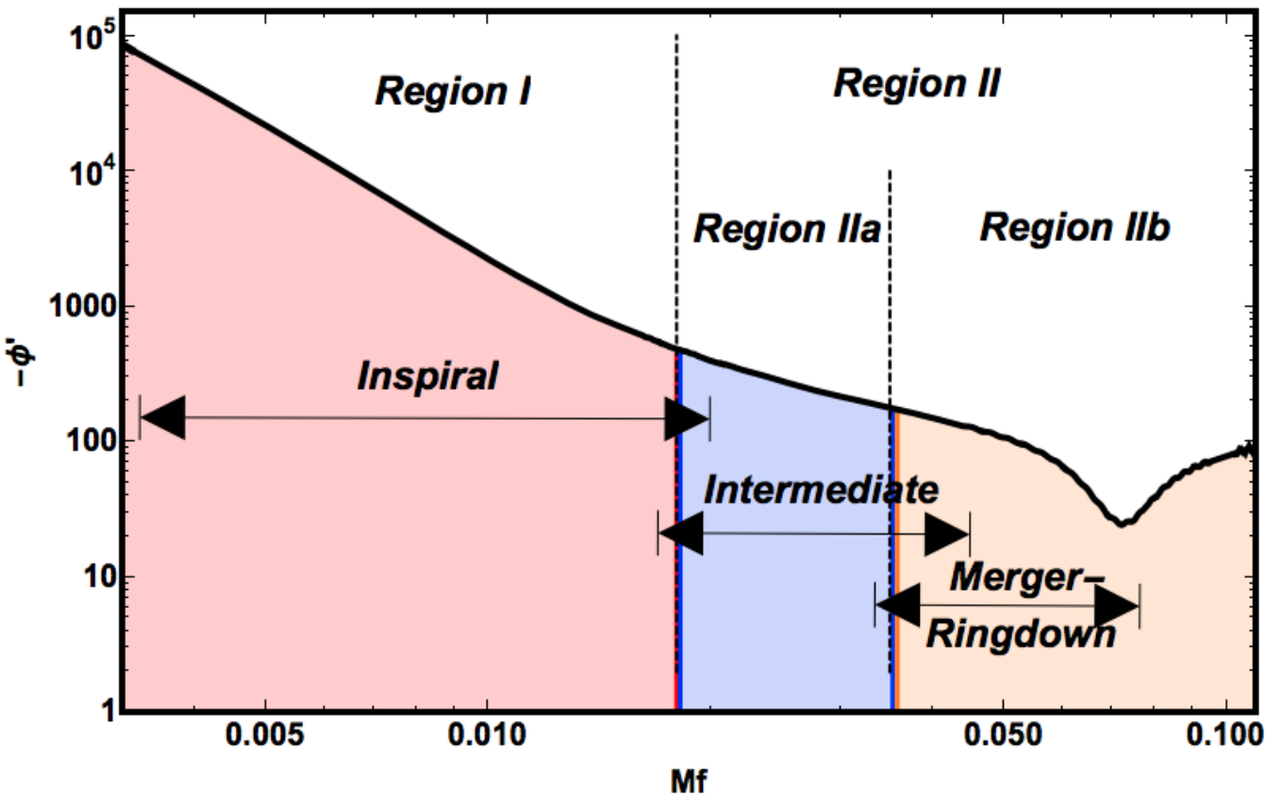

On phenomenological inspiral-merger-ringdown waveforms

(Santamaria, Ohme et al. 10)

$$\tilde{h}(f;\lambda_i) = \mathcal{A}(f;\lambda_i)\, e^{i\phi(f;\lambda_i)}$$

$$\mathcal{A}(f;\lambda_i) \equiv C \begin{cases} \left(\frac{\pi M f}{a_0\nu^2+b_0\nu+c_0}\right)^{-7/6} & \text{if } f < \frac{a_0\nu^2+b_0\nu+c_0}{\pi M} \\ \left(\frac{\pi M f}{a_0\nu^2+b_0\nu+c_0}\right)^{-2/3} & \text{if } \frac{a_0\nu^2+b_0\nu+c_0}{\pi M} \le f < \frac{a_1\nu^2+b_1\nu+c_1}{\pi M} \\ w\,\mathcal{L}\left(f, \frac{a_1\nu^2+b_1\nu+c_1}{\pi M}, \frac{a_2\nu^2+b_2\nu+c_2}{\pi M}\right) & \text{if } \frac{a_1\nu^2+b_1\nu+c_1}{\pi M} \le f < \frac{a_3\nu^2+b_3\nu+c_3}{\pi M} \end{cases}$$

$$\phi(f;\lambda_i) = 2\pi f t_0 + \varphi_0 + \frac{1}{\nu}\sum_{k=0}^{7}(x_k\,\nu^2 + y_k\,\nu + z_k)\,(\pi M f)^{(k-5)/3}$$

- Extended to **spin effects**, including **effective precession**.

(Khan et al. 15; Husa et al. 15; Hannam et al. 13)

Spinning precessing waveform models

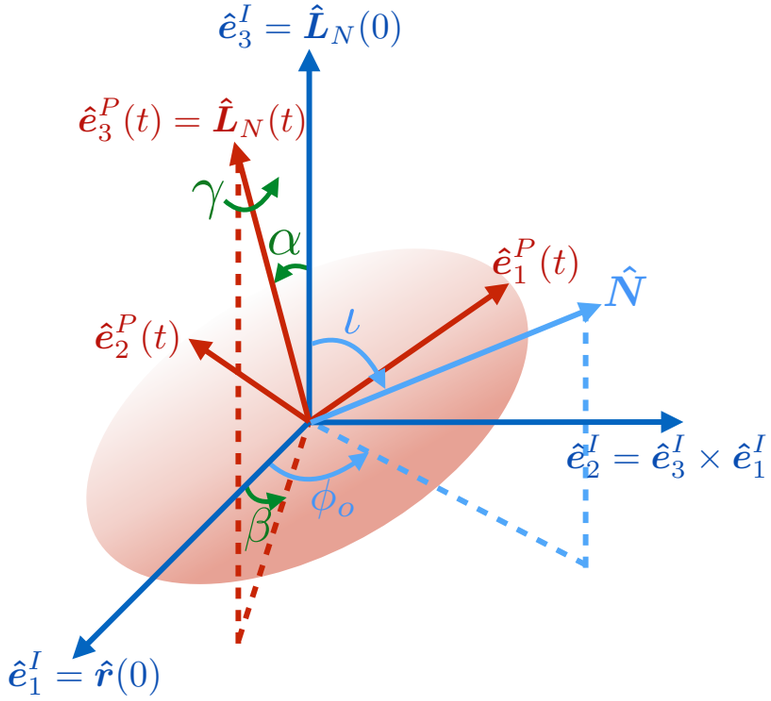

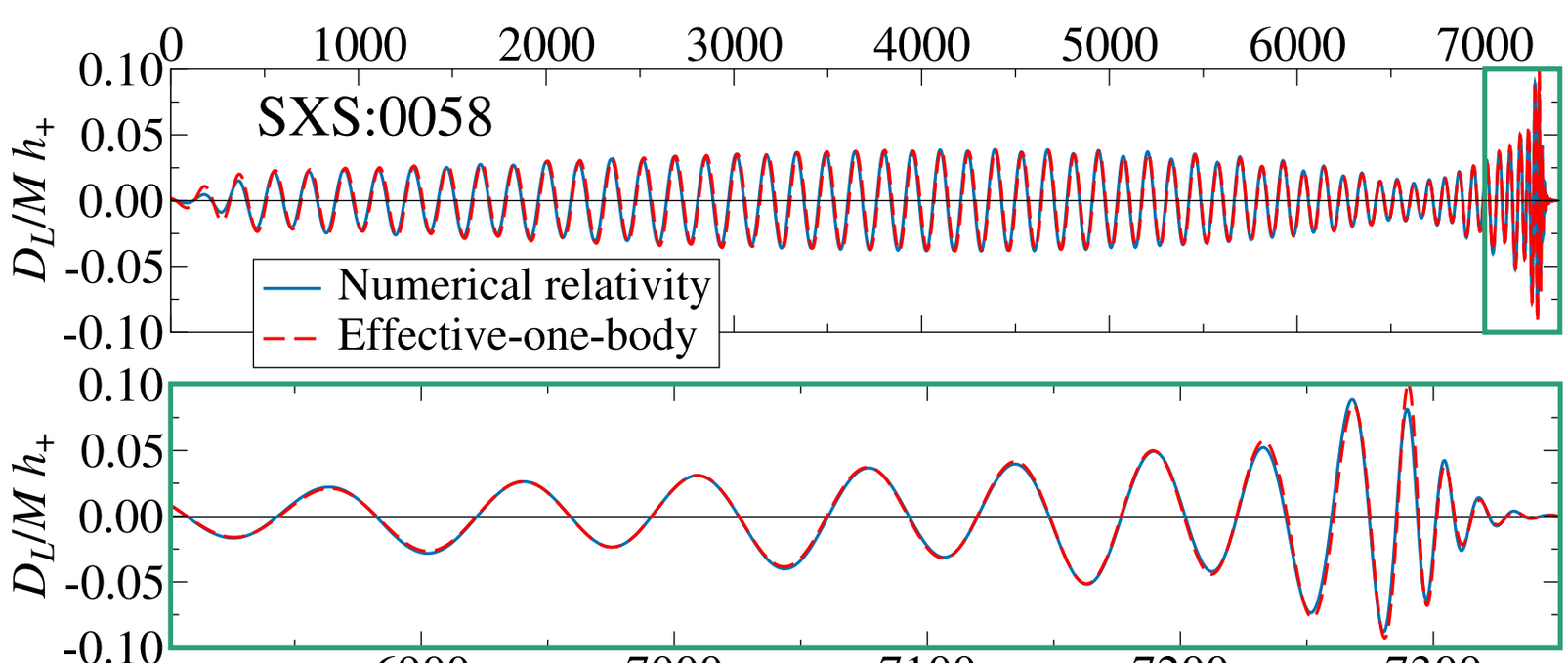

Precessing (co-rotating) frame
(AB, Chen & Vallisneri 03, Boyle et al. 11, Schmidt et al. 11, O'Shaughessy et al. 11)

(Pan et al. 14, Babak et al. 16)

- **Single** effective-**spin precessing** waveform model in **frequency domain** (IMR phenomenological, 13-independent parameters). *(Schmidt et al. 12, Hannam et al. 14)*

- **Double-spin precessing** waveform model in **time domain** (EOBNR, 15-independent parameters). *(Pan et al. 14, Babak et al. 16)*

Detection confidence with modeled search in O2

- **Matched filtering** employed

(Dal Canton & Harry 17)

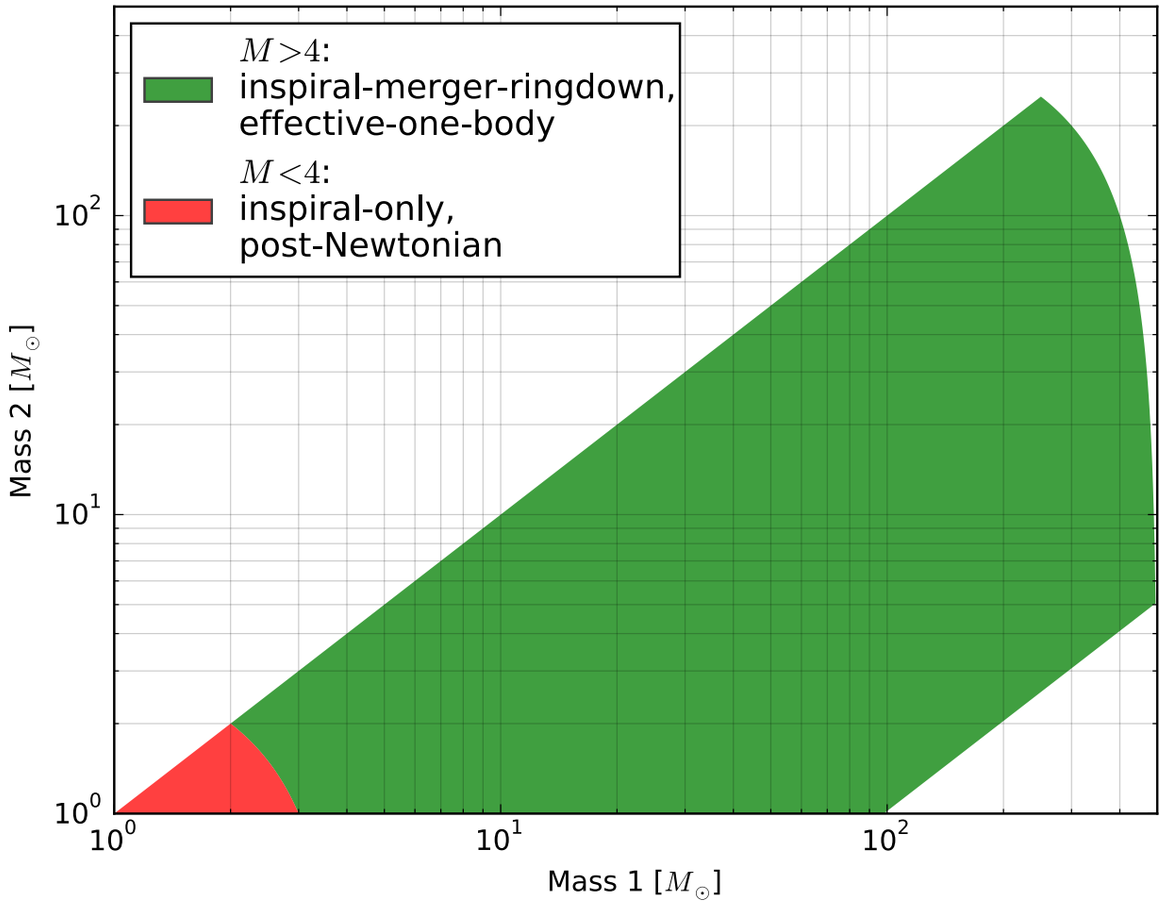

only (2,2) & (2,-2) modes use in templates

(Abbott et al. PRL 118 (2017) 221101)

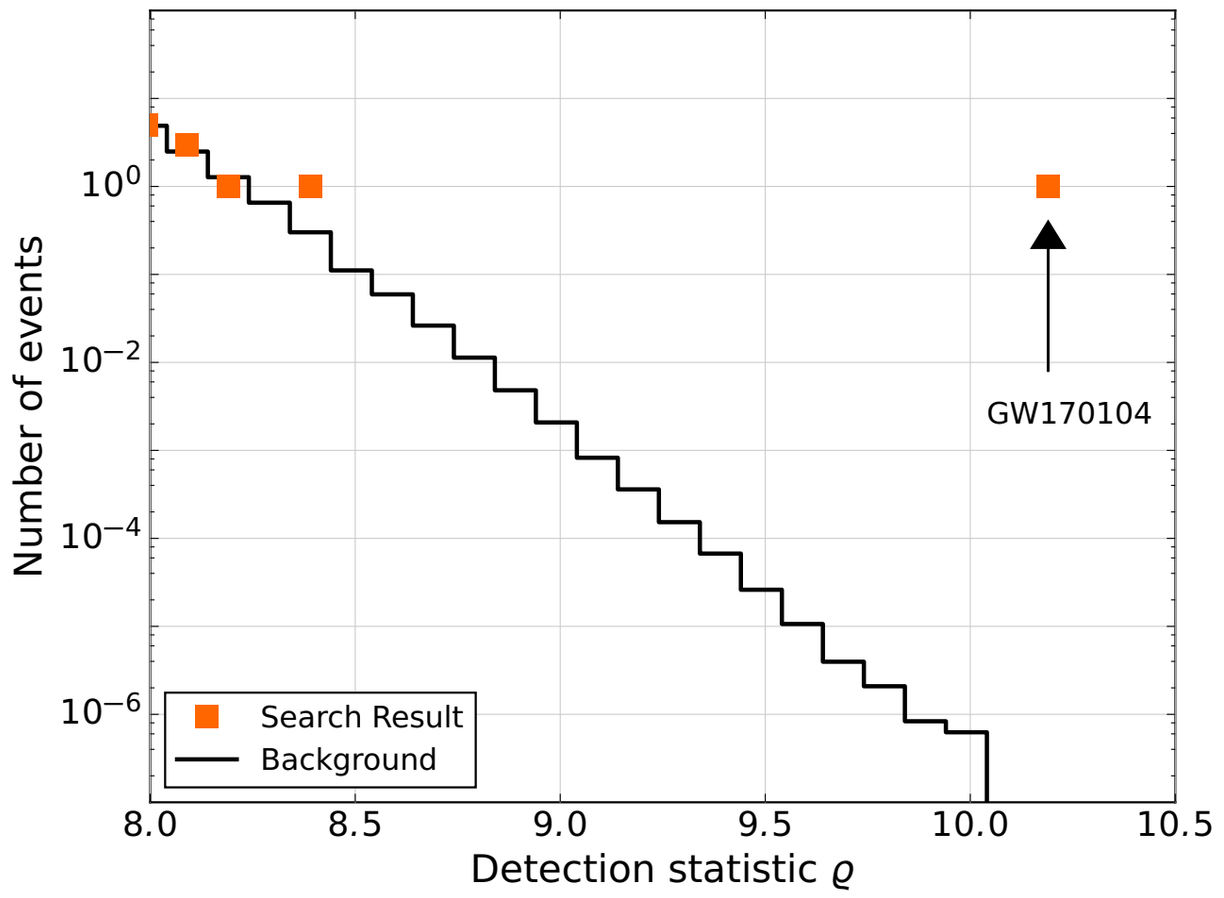

- **Modeled-search:** at detection statistic value of **GW170104, GW170814, GW170608, false alarm rate** is **less than 1 in 70000, 40000, 3000 years** of coincident observing time.
- **Modeled-search:** false alarm rate is **less than 1 in 80,000 years for GW170817.**

Detection confidence with modeled search in O2 (contd.)

- **Matched filtering** employed

$$\hat{d} = \int_{-\infty}^{\infty} dt\, K(t)\, d(t)$$

filter

data noise signal

$$d(t) = n(t) + h(t)$$

$S =< \hat{d} >$ ← expectation value over several noise realizations/time average

$$N = \sqrt{(< \hat{d}^2 > - < \hat{d} >^2)}_{|h=0}$$ ← variance when signal is absent

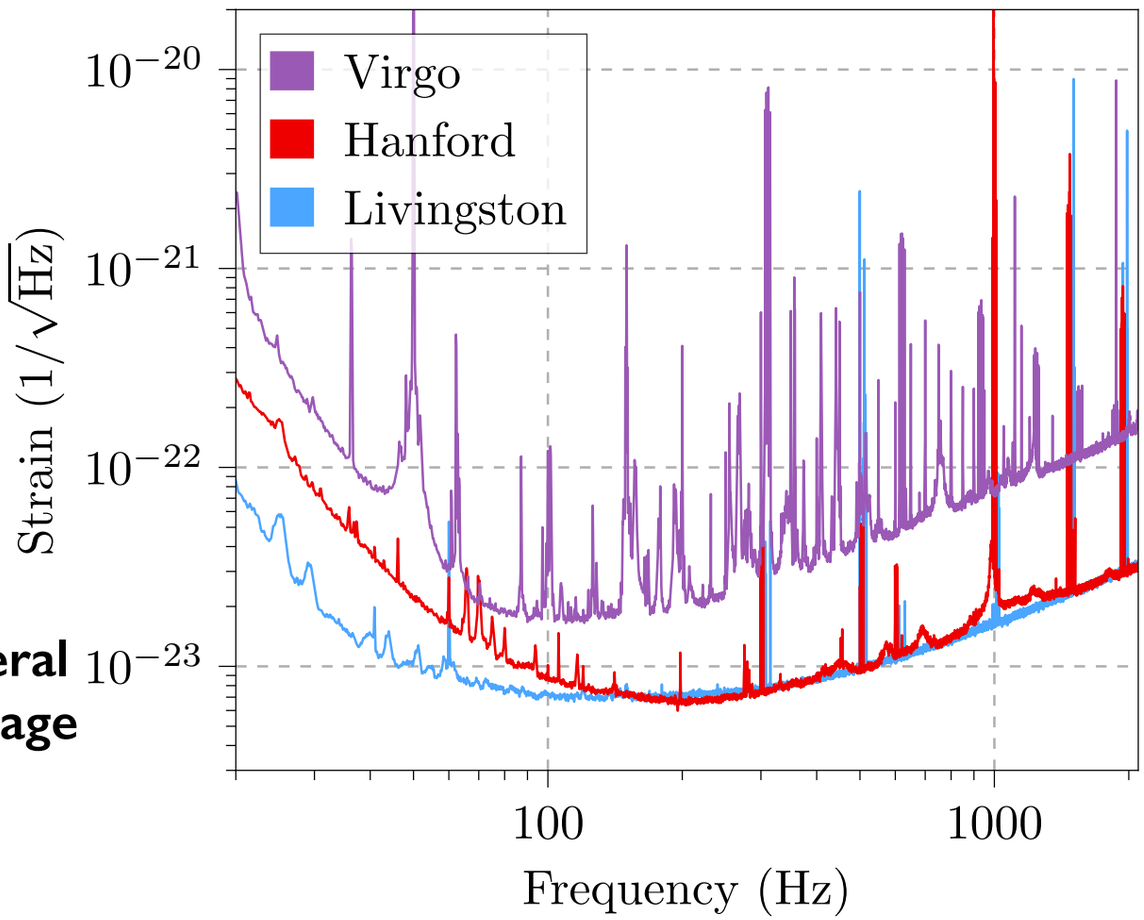

(Abbott et al. PRL 119 (2017) 141101)

- Optimal SNR: $\left(\frac{S}{N}\right) = \sqrt{(h|h)}$

- Optimizing SNR: $\tilde{K}(f) \propto \frac{\tilde{h}(f)}{S_n(f)}$

$$(h_1|h_2) = 4\mathrm{Re}\int_0^{\infty} df\, \frac{\tilde{h}_1^*(f)\,\tilde{h}_2(f)}{S_n(f)}$$

- Statistics: $\rho = \frac{\hat{d}}{N}$

Assessing confidence in LIGO detection

Could the **signal** be **due** to **noise fluctuations**?

(animation by Nuttall)

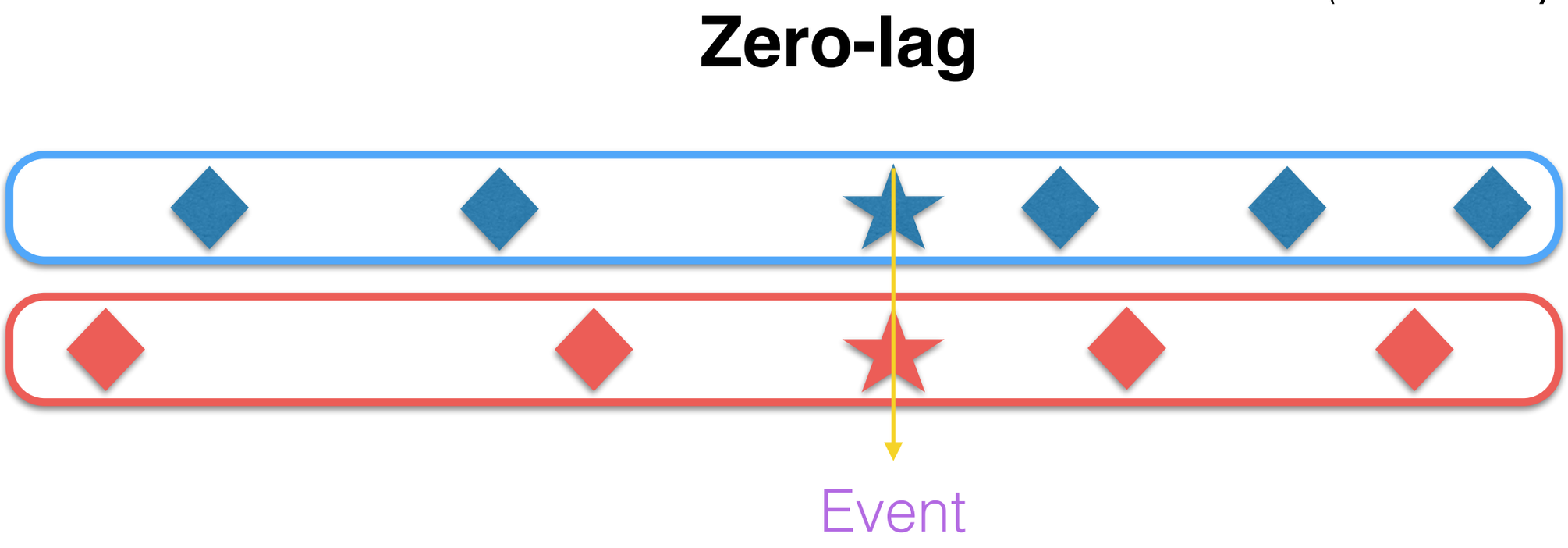

Assessing confidence in LIGO detection

Building larger background by time-shifting the data

(animation by Nuttall)

Zero-lag

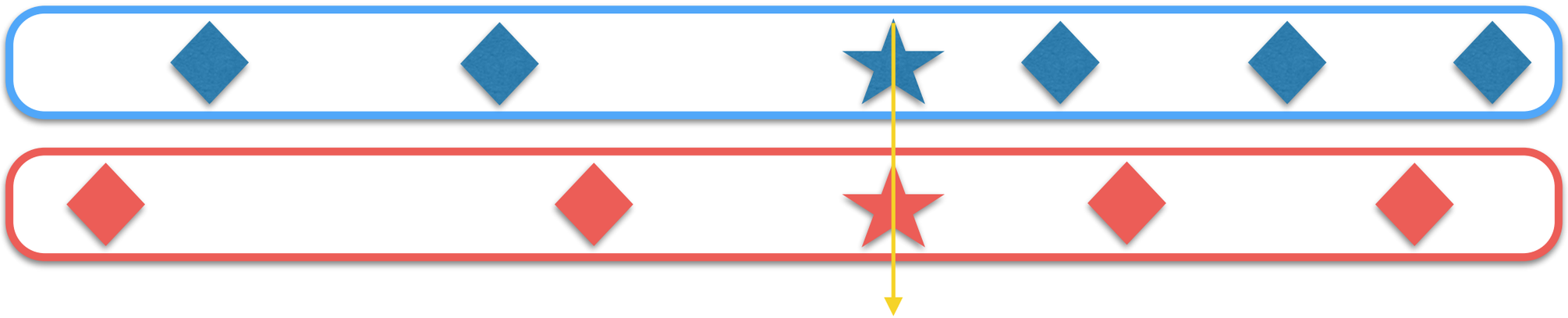

Event

Time slide

Background event

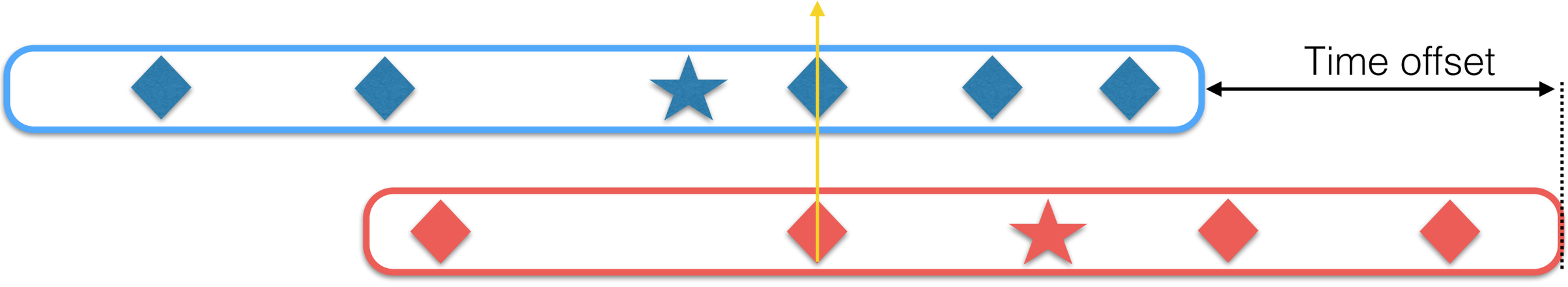

Assessing confidence in LIGO detection

Building larger background by time-shifting the data

(animation by Nuttall)

Zero-lag

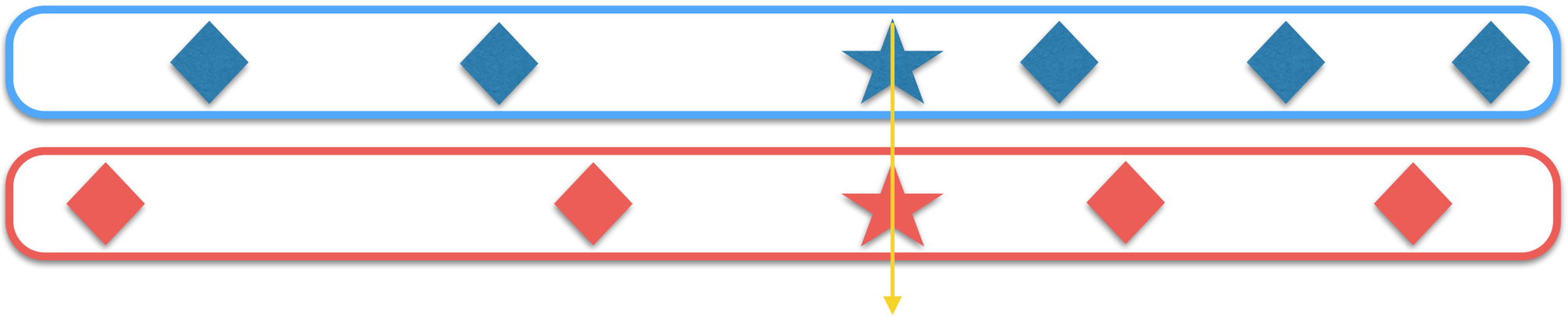

Event

Time slide

Background event

Event + background

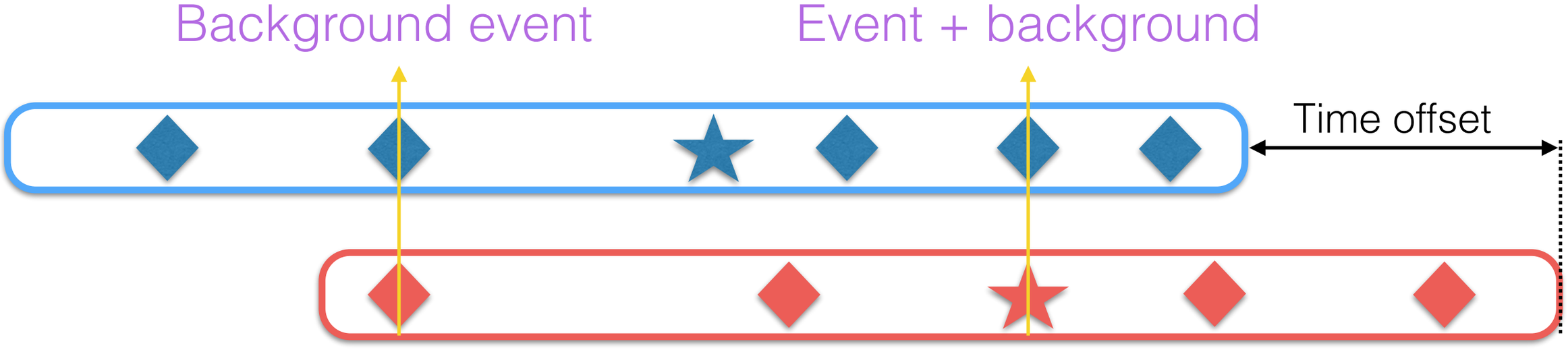

Assessing confidence in LIGO detection for GW150914

(*Abbott et al.* Phys.Rev. X6 (2016) no.4, 041015)

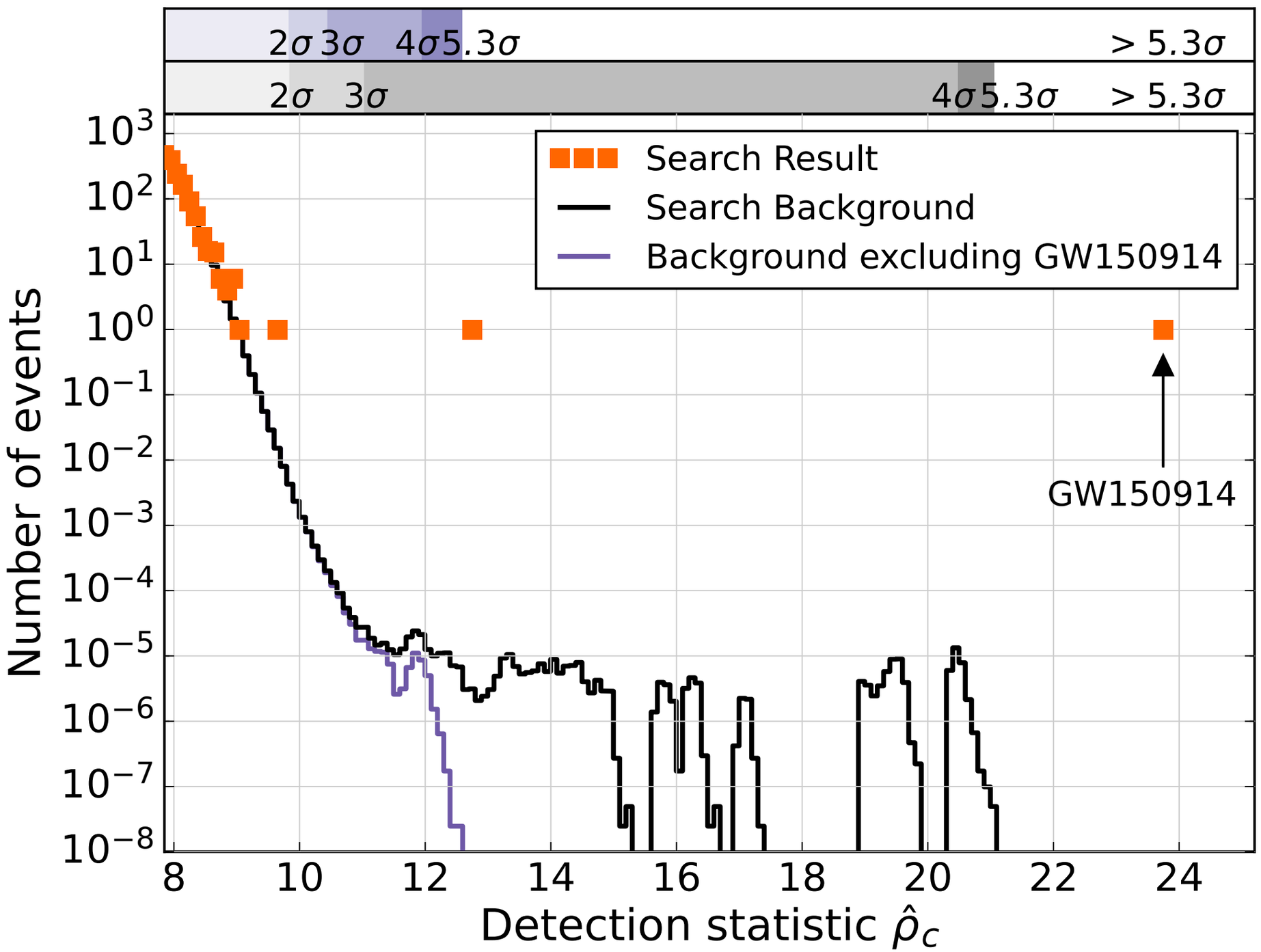

Assessing possible modeling systematics of GW events

(visualization credit: Dietrich, Haas @AEI)

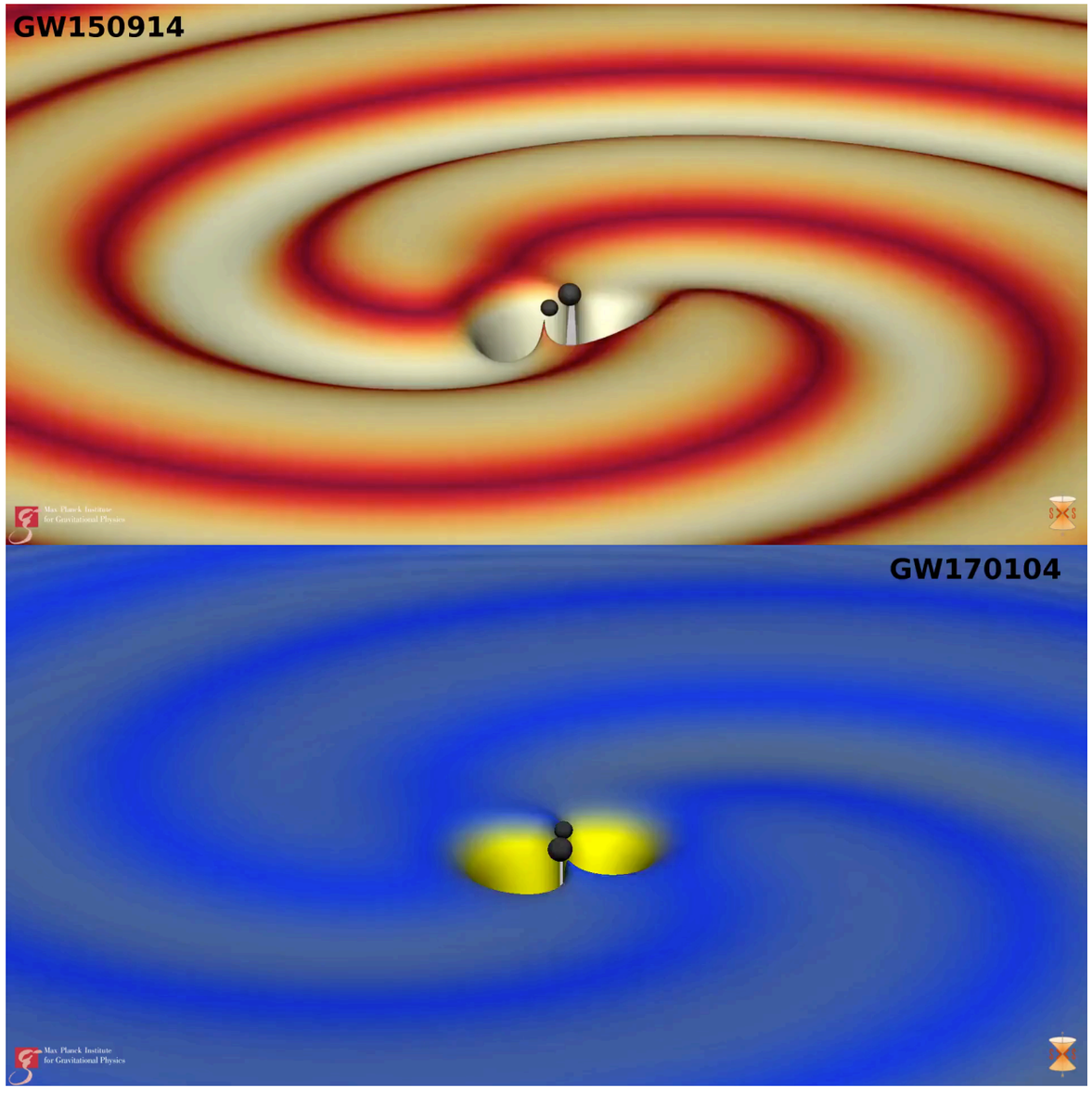

$$M_\odot = 60\text{–}70M_\odot \qquad M_\odot = 46\text{–}57M_\odot$$

(Ossokine, AB & SXS project)

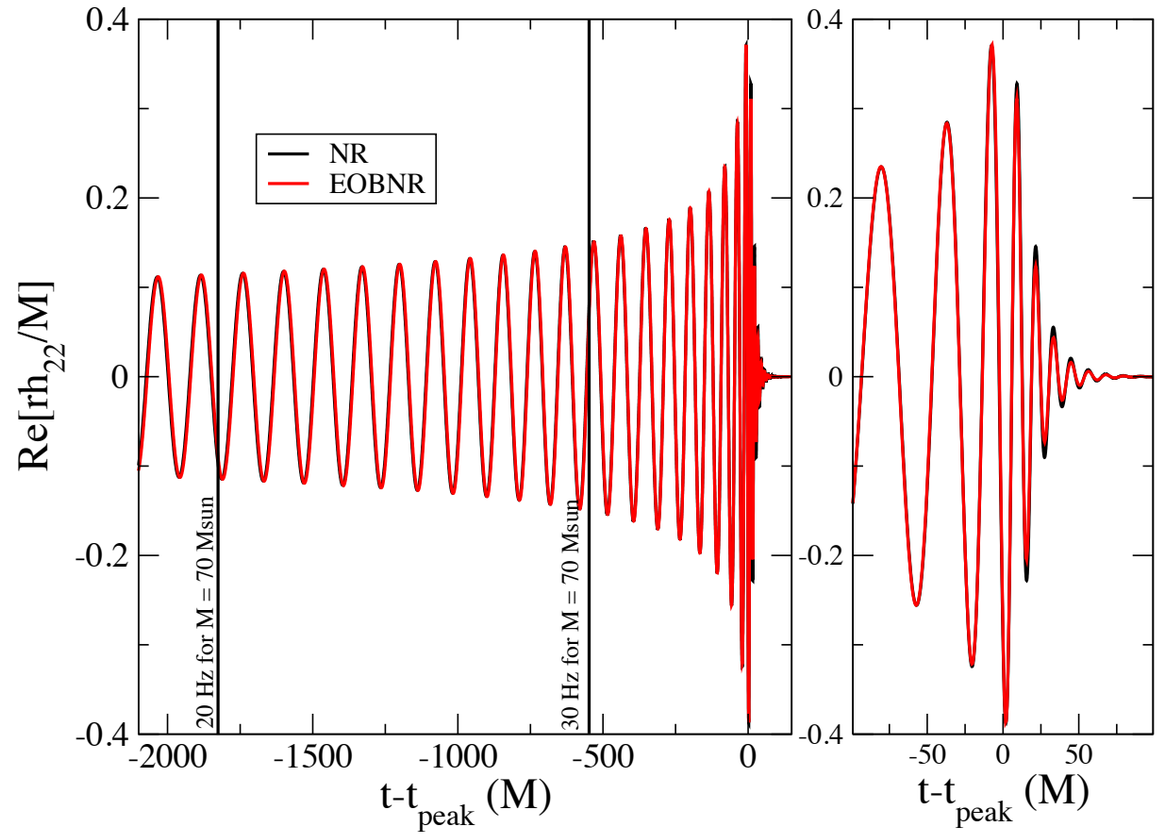

- **Systematics** due to modeling **are smaller than statistical** errors.

(see also Abbott et al. CQG 34 (2017) 104002)

Assessing possible modeling systematics of GW events

(visualization credit: Dietrich, Haas @AEI)

(Ossokine, AB & SXS project)

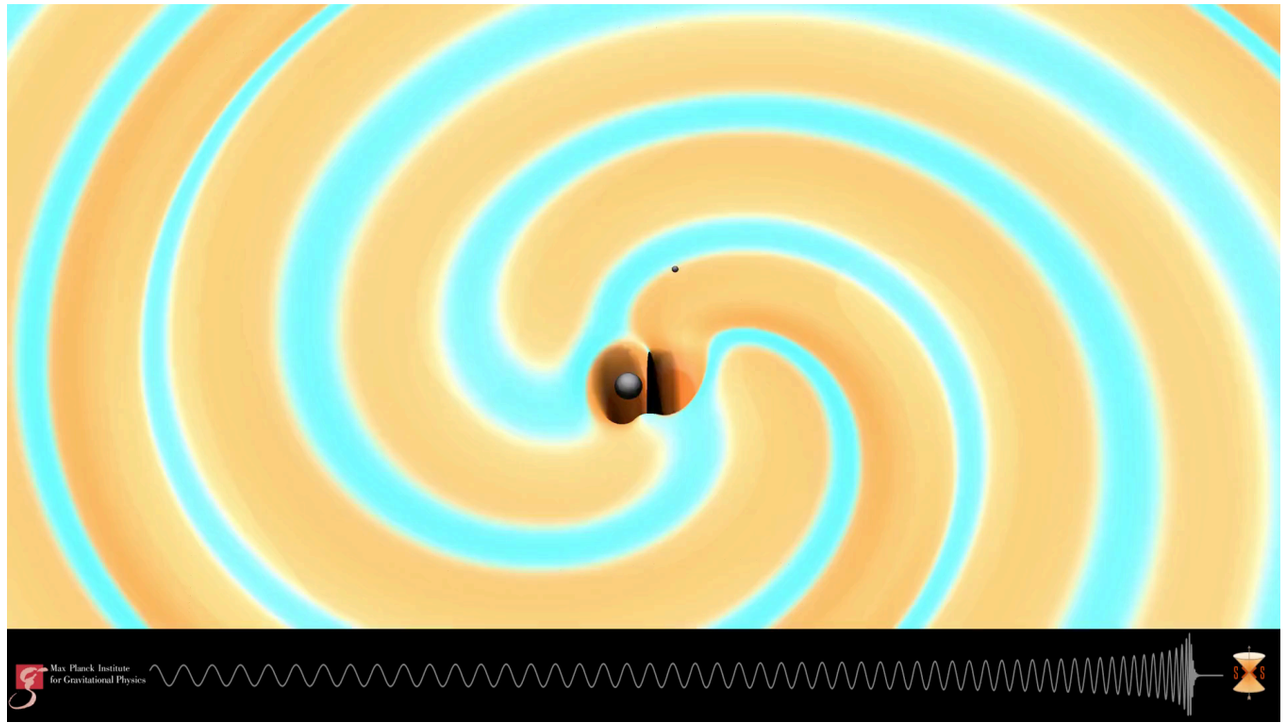

(Abbott et al. PRL 116 (2016) 241103)

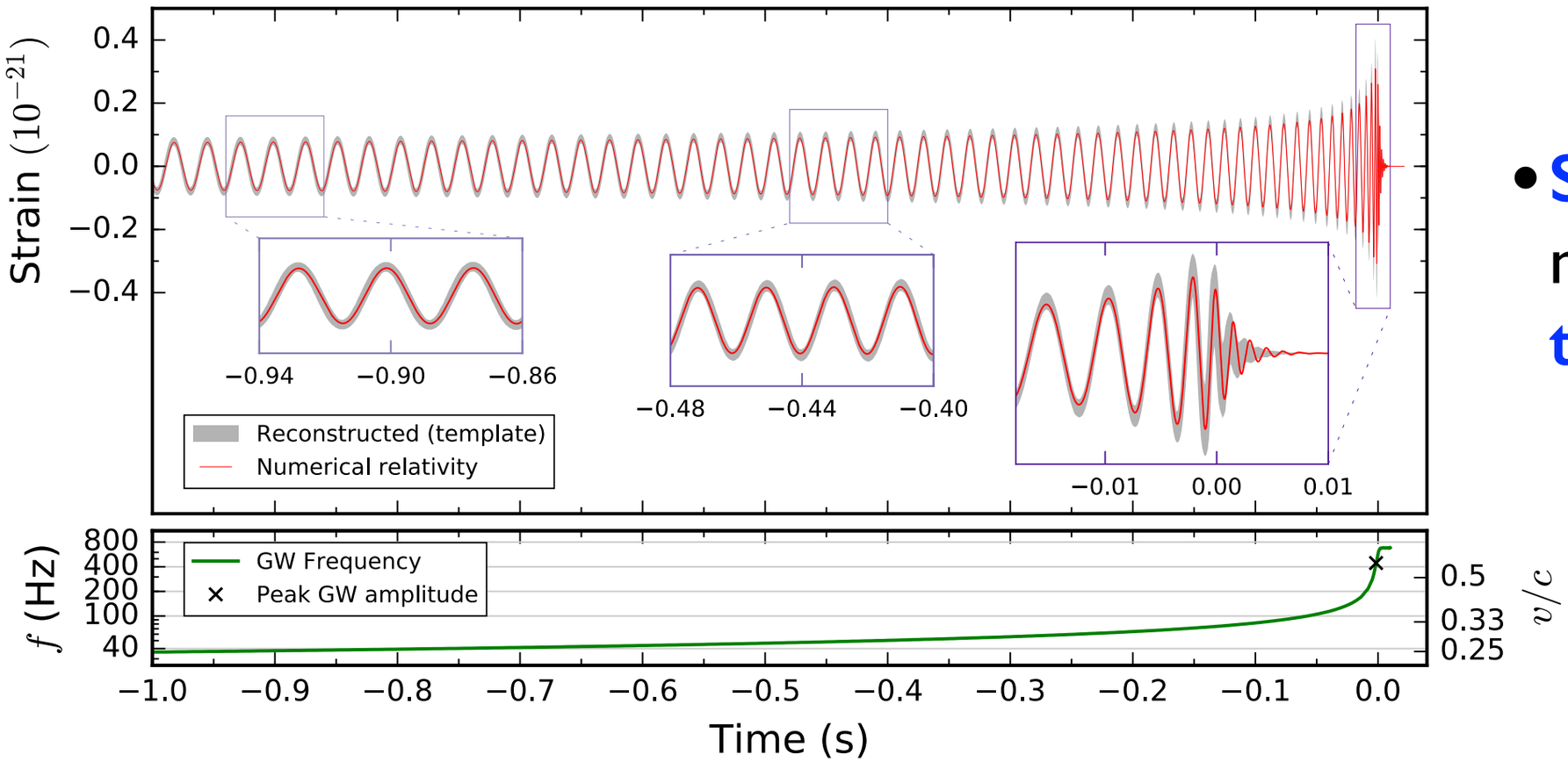

- **Systematics** due to modeling **are smaller than statistical** errors.

(see also Abbott et al. CQG 34 (2017) 104002)

On systematics due to modeling comparing to NR waveform

- **Mock signal** from NR simulation with parameters close to GW150914.

(Abbott et al. CQG 34 (2017) 104002)

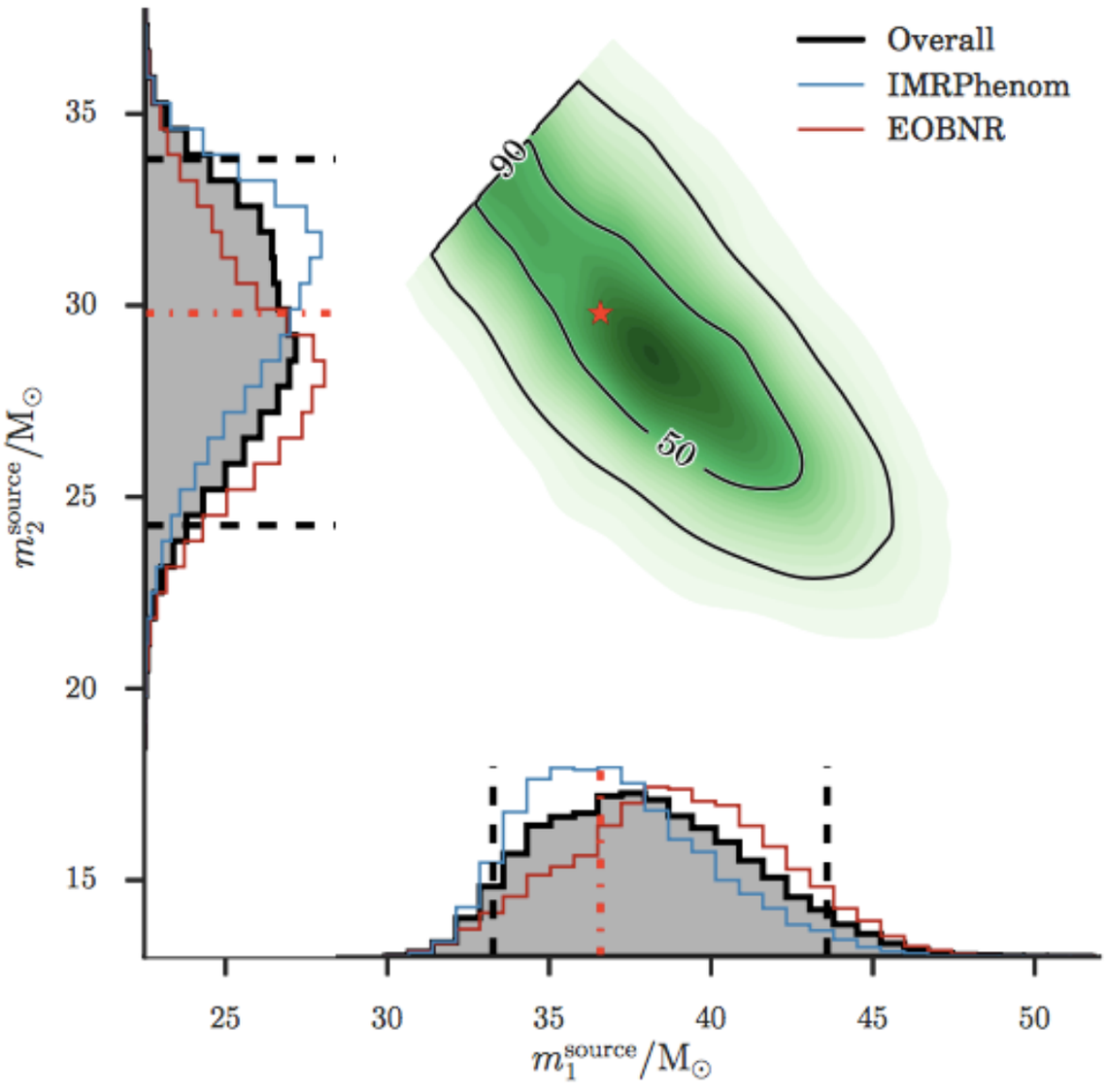

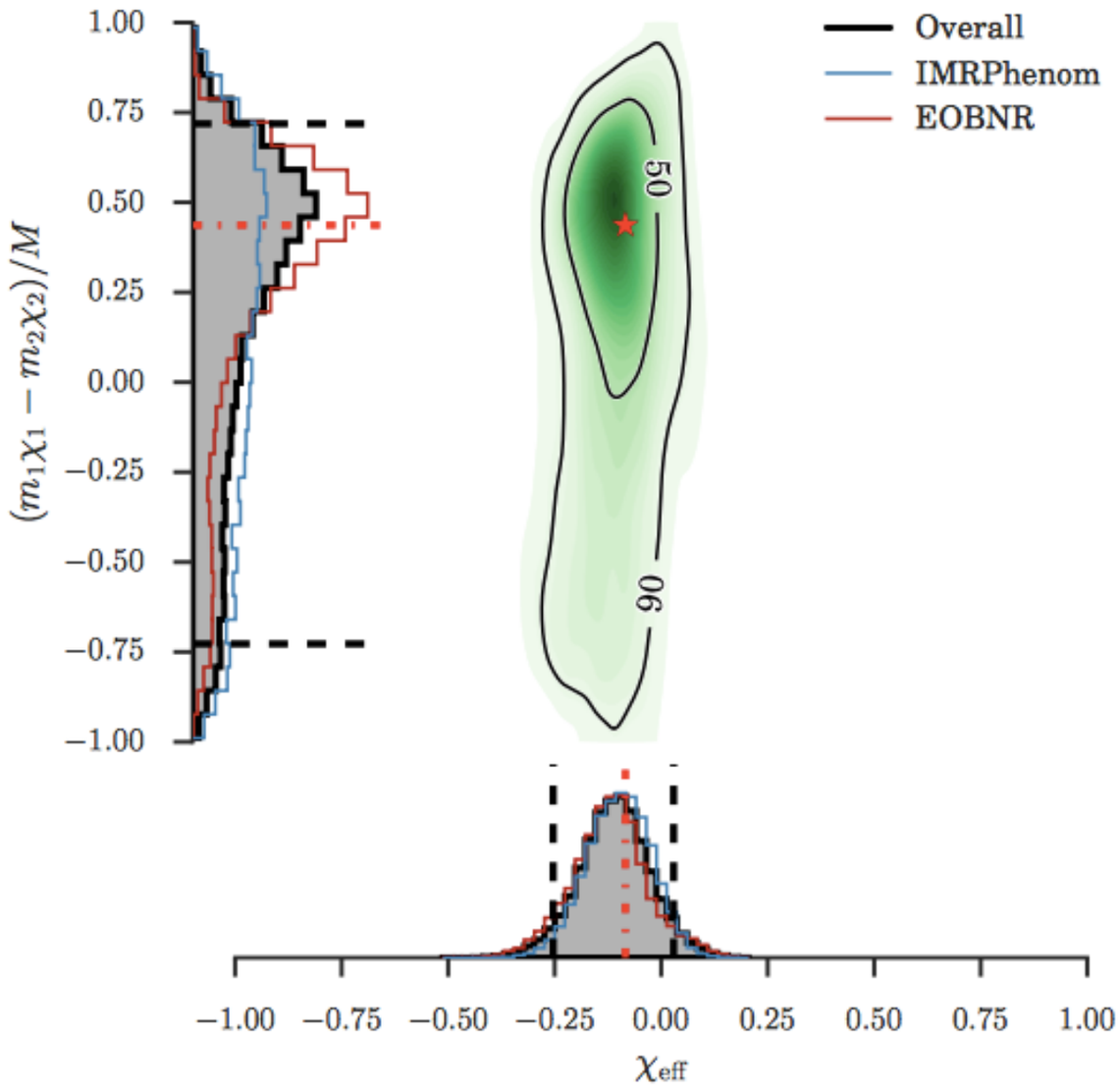

- **Overall, no evidence for systematic bias** relative to the statistical error of original parameter recovery of GW150914.

On systematics due to modeling comparing to NR waveform (contd.)

(Abbott et al. CQG 34 (2017) 104002)

- **Parameter biases** are found to occur for some **configurations disfavored by data** of GW150914.

- E.g., biases are present for **binaries inclined edge-on to the detector** over a small range of choices of polarization angles.

(see also Williamson et al. 2017)

- Biases can be present for **binaries with eccentricity > 0.05**.

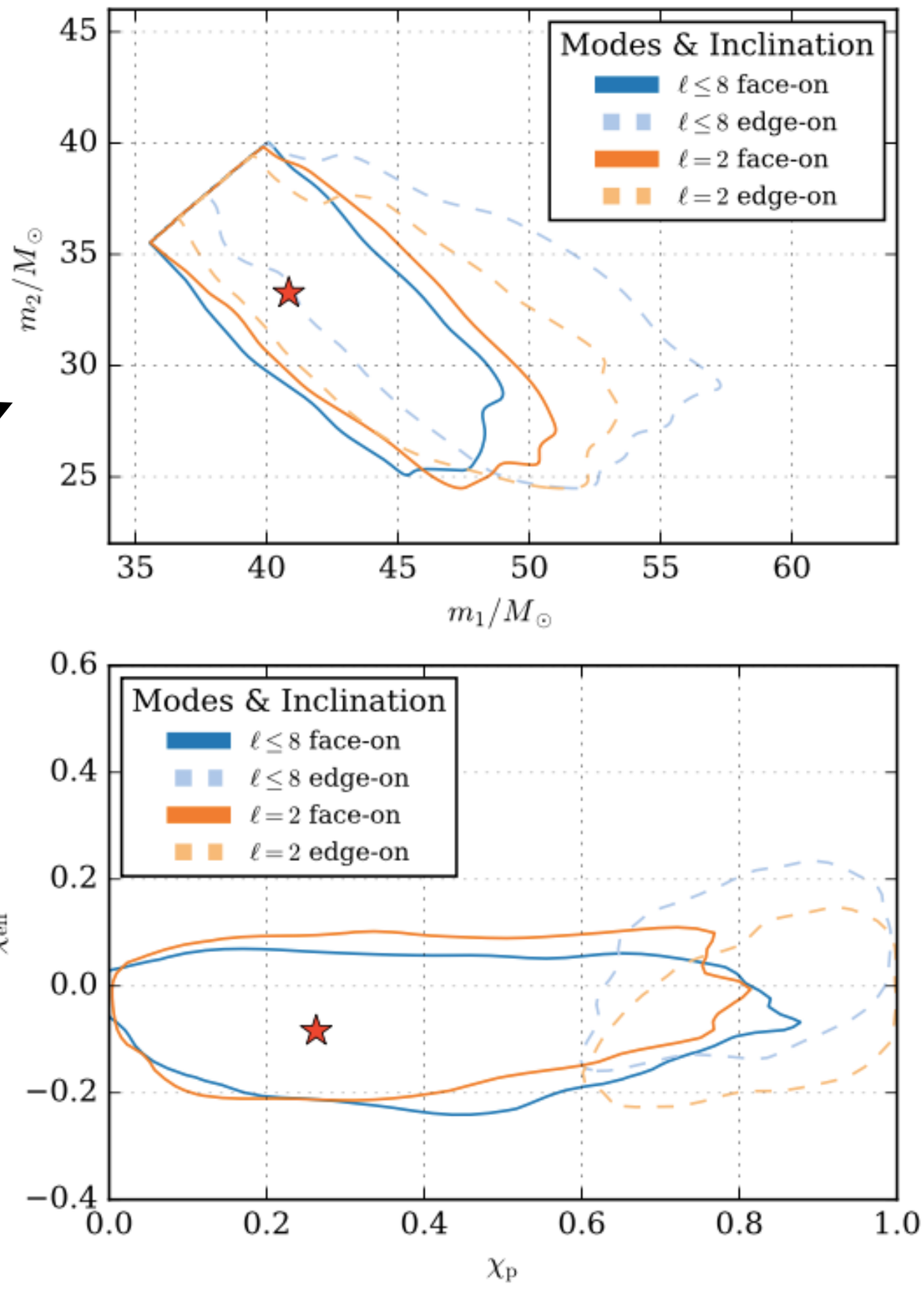

Comparing EOBNR & IMRPhenom models: detection

- **Aligned/anti-aligned** waveform models. Only dominant **(2,2) mode**.

Effectualness *(Bohe',…, AB et al. 16)*

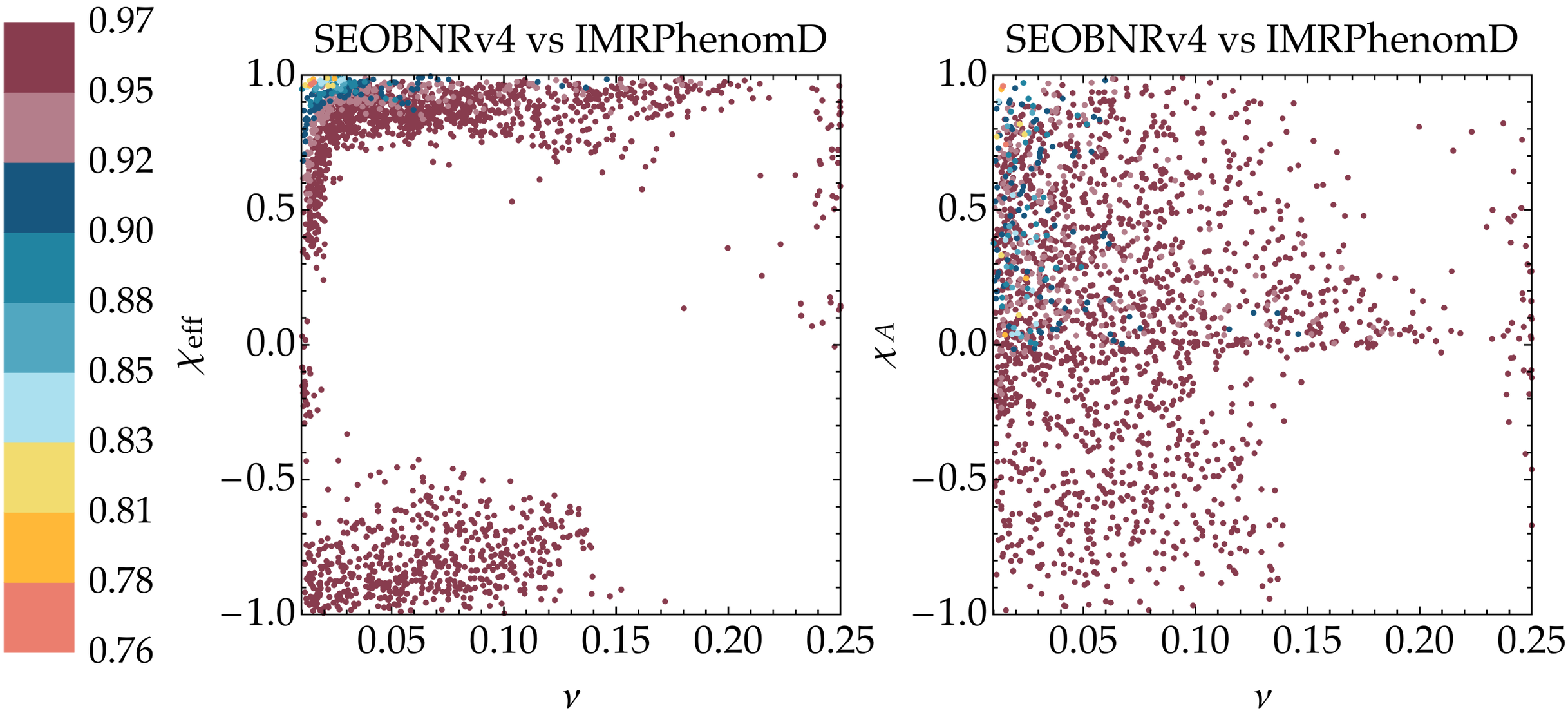

[Note that only 2.1% of 100,000 points have matches < 97%.]

Comparing EOBNR & IMRPhenom models: inferring parameters

- **Aligned/anti-aligned** waveform models. Only dominant **(2,2) mode**.
- Differences for **large mass ratios** (> 4) **and large spins** (> 0.8).

Faithfulness *(Bohe',…, AB et al. 16)*

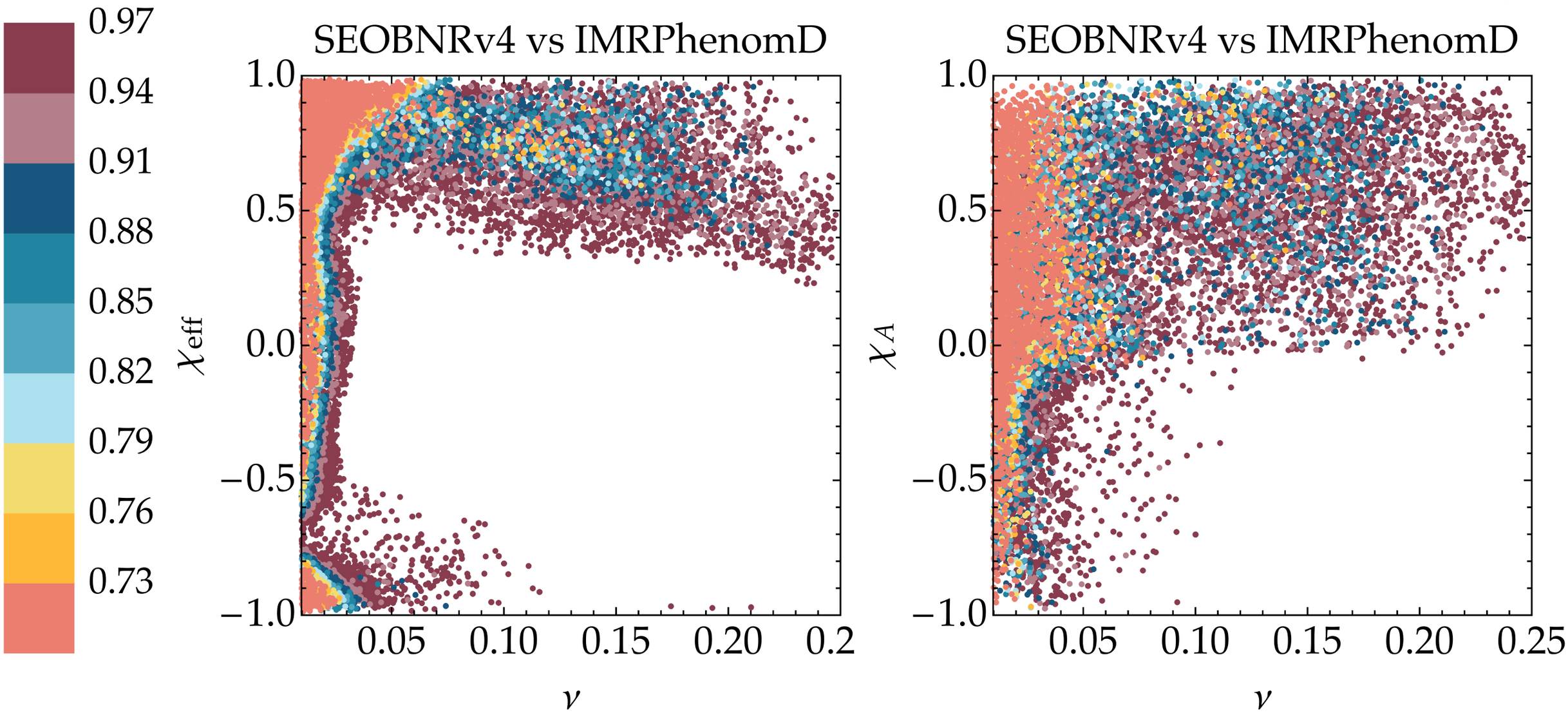

[Note that only 7% of 200,000 points have matches < 97%.]

Extending waveform model in all BBH parameter space

- Difficult to run **NR simulations** for **large mass ratios** (> 4) **and large spins** (> 0.8), with **large number** of GW **cycles** (> 50).

(Bohe',…, AB et al. 16)

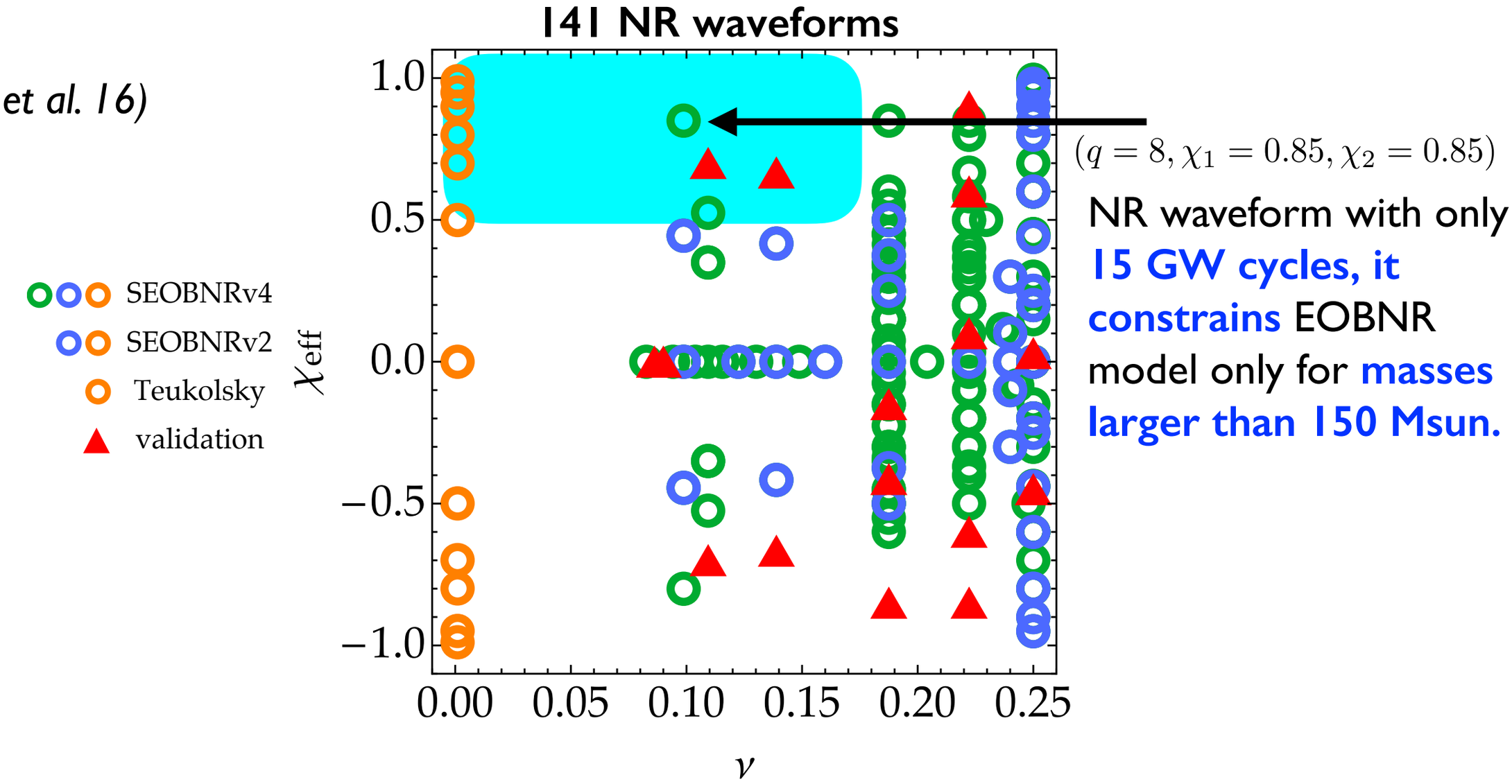

NR waveform with only **15 GW cycles, it constrains** EOBNR model only for **masses larger than 150 Msun.**

- For large mass ratios (> 4) combine **PN & GSF** results in **EOB** framework.
  (Damour 09; Barausse et al. 12, Le Tiec et al. 12, Bini et al. 12-16, Antonelli et al. in progress)
- Inclusion of **GSF** also important for **EMRIs** (LISA) and **IMRIs** (3G detectors).

Inferring sources' properties/model selection upon detection

- **Bayes theorem**:

Likelihood function ↓ ↓ prior probability

$$\mathcal{P}(\theta|d,\mathcal{H}) \propto \Lambda(d|\theta,\mathcal{H}) \times \mathcal{P}(\theta,\mathcal{H})$$

↑

posterior probability distribution

- **Likelihood function** for observed data d(t) = n(t) + h(t), given hypothesis that there is GW signal with parameters θ :

$$\Lambda(d|\theta,\mathcal{H}) \propto \exp\left(-2\sum_i \frac{|\tilde{d}(f_i) - \tilde{h}(f_i;\theta)|^2}{S_n(f_i)}\right)$$

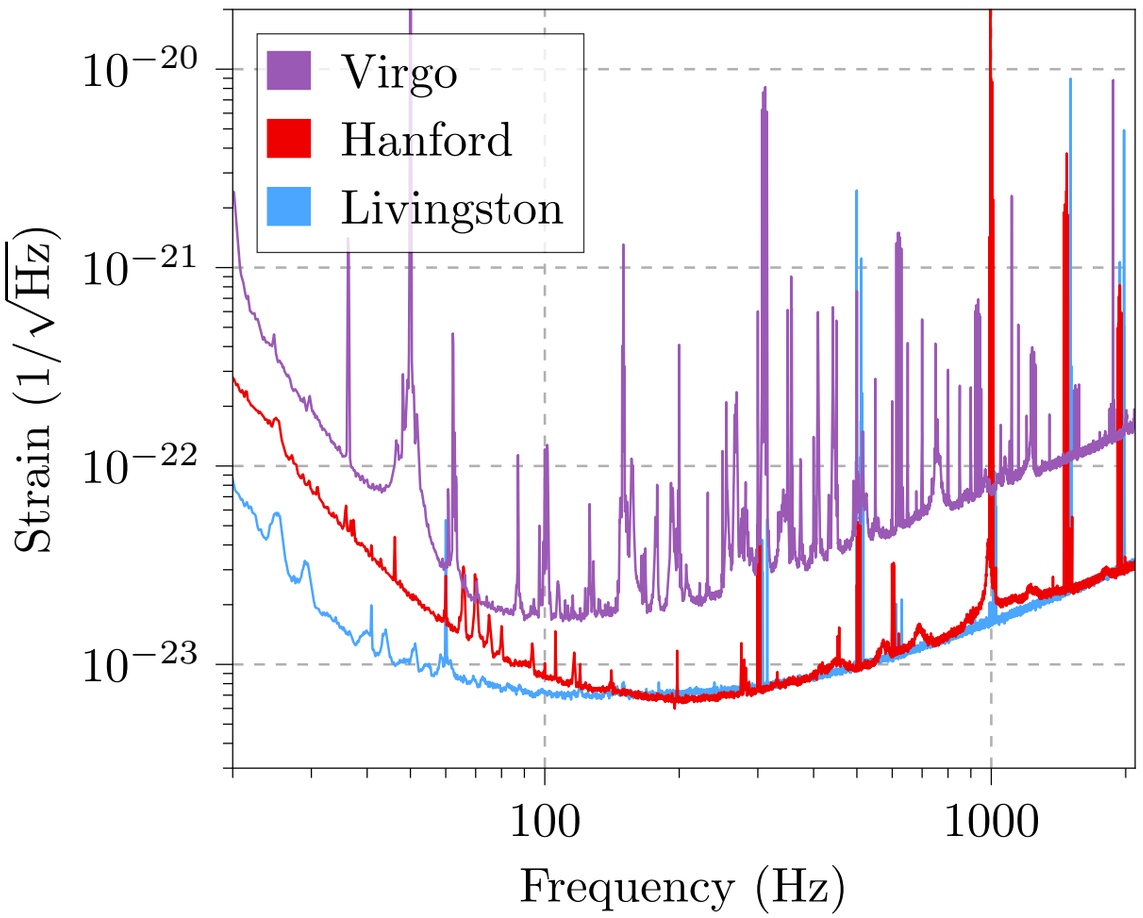

(Abbott et al. PRL 119 (2017) 141101)

Inferring sources' properties/model selection upon detection

- **Bayes theorem**:

Likelihood function ↓ ↓ prior probability

$$\mathcal{P}(\theta|d,\mathcal{H}) \propto \Lambda(d|\theta,\mathcal{H}) \times \mathcal{P}(\theta,\mathcal{H})$$

↑ posterior probability distribution

- **Likelihood function** for observed data d(t) = n(t) + h(t), given hypothesis that there is GW signal with parameters θ :

$$\Lambda(d|\theta,\mathcal{H}) \propto \exp\left(-2\sum_i \frac{|\tilde{d}(f_i) - \tilde{h}(f_i;\theta)|^2}{S_n(f_i)}\right)$$

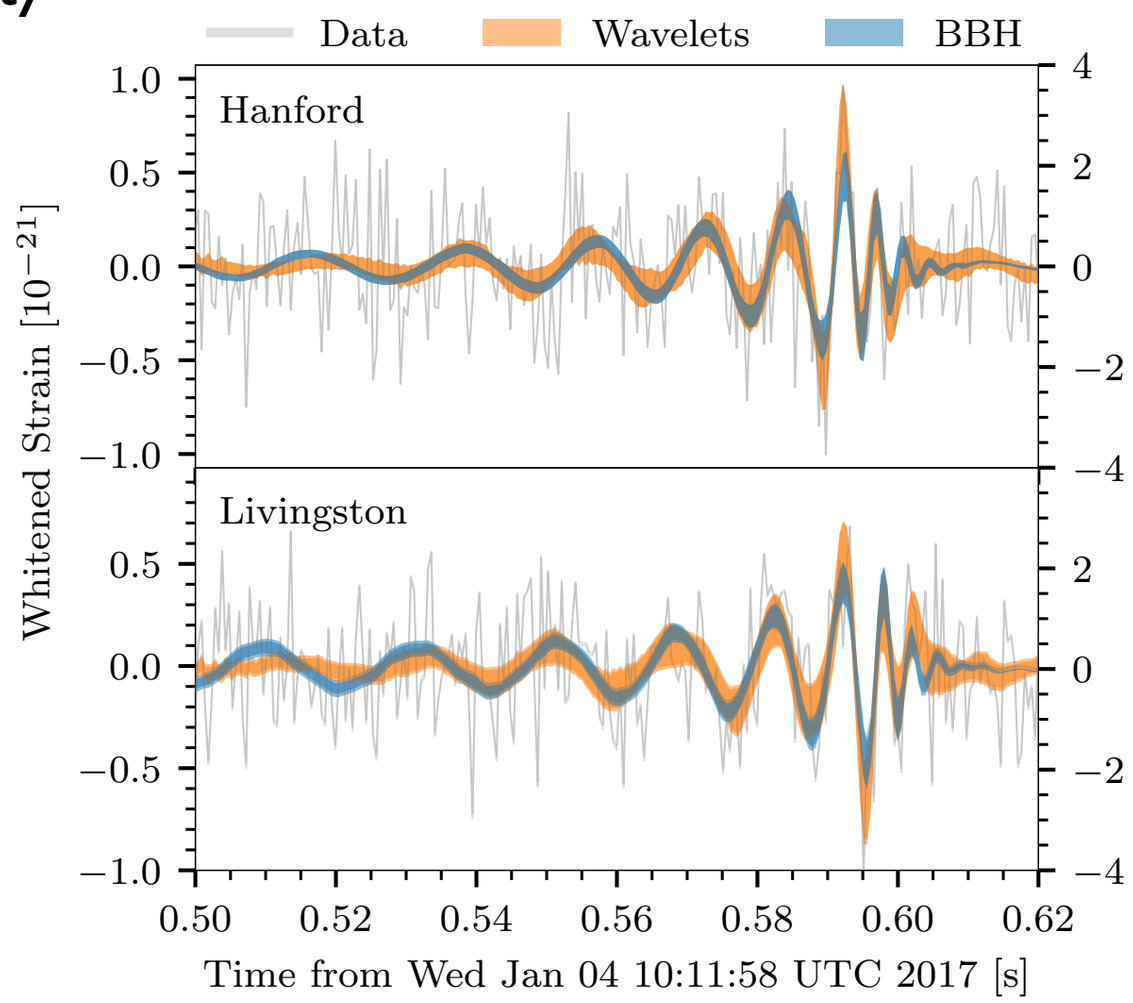

(Abbott et al. PRL 118 (2017) 221101)

- Subtracting **best-fit GR waveform** model (MaP) from data

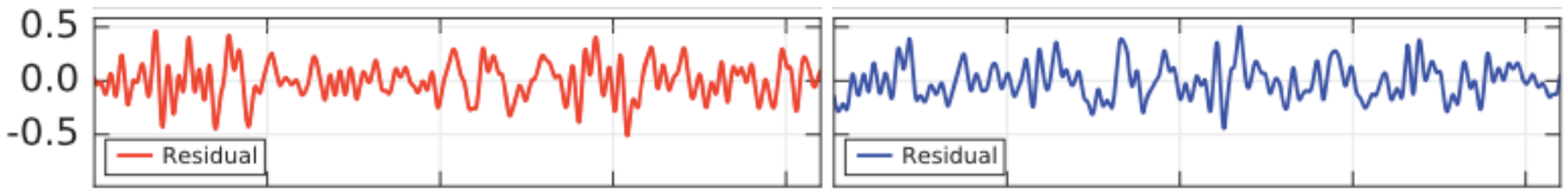

Unveiling binary black-hole properties: masses

(Abbott et al. PRL 118 (2017) 221101)

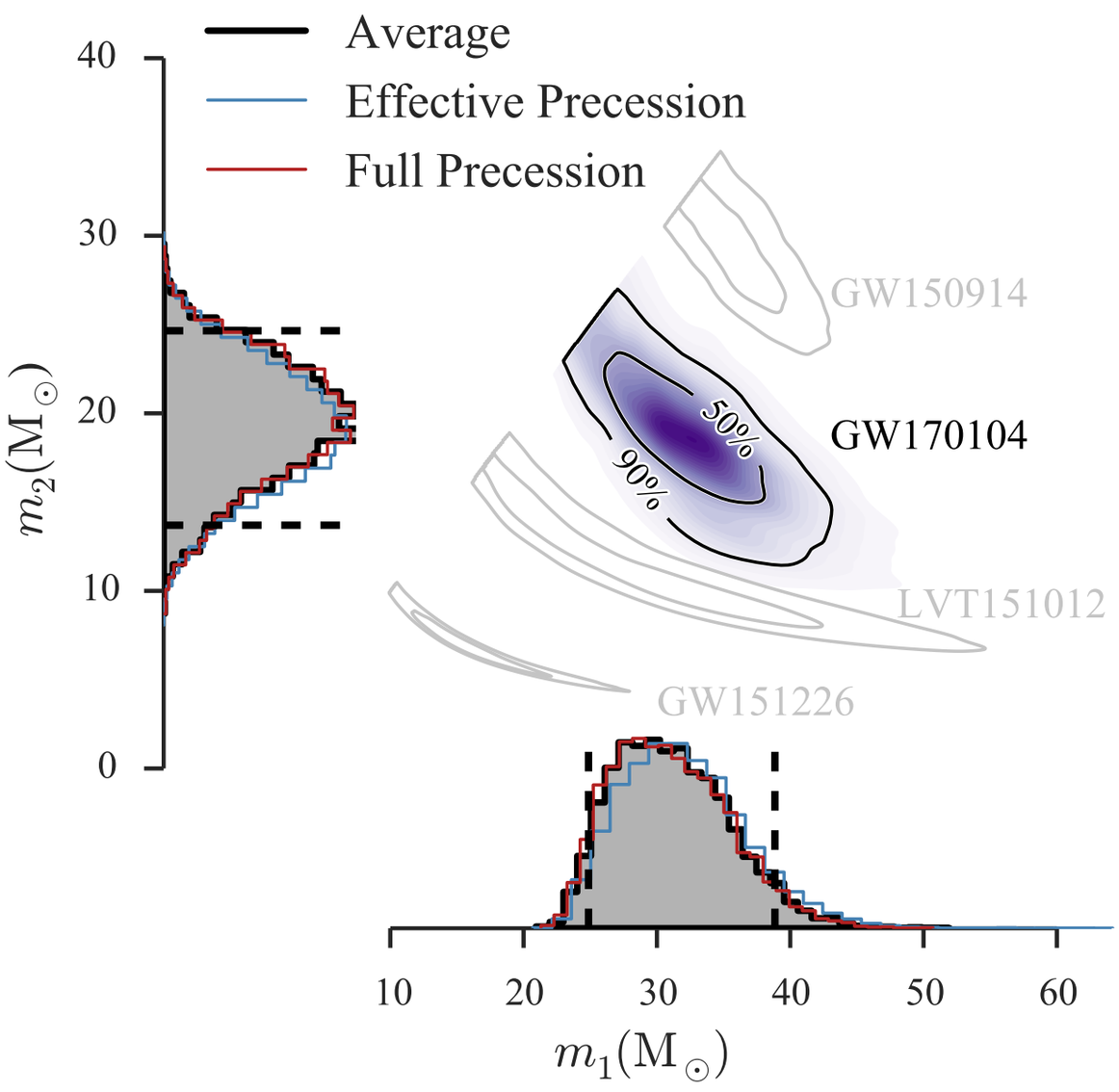

(Abbott et al. ApJ 851 (2017) L35)

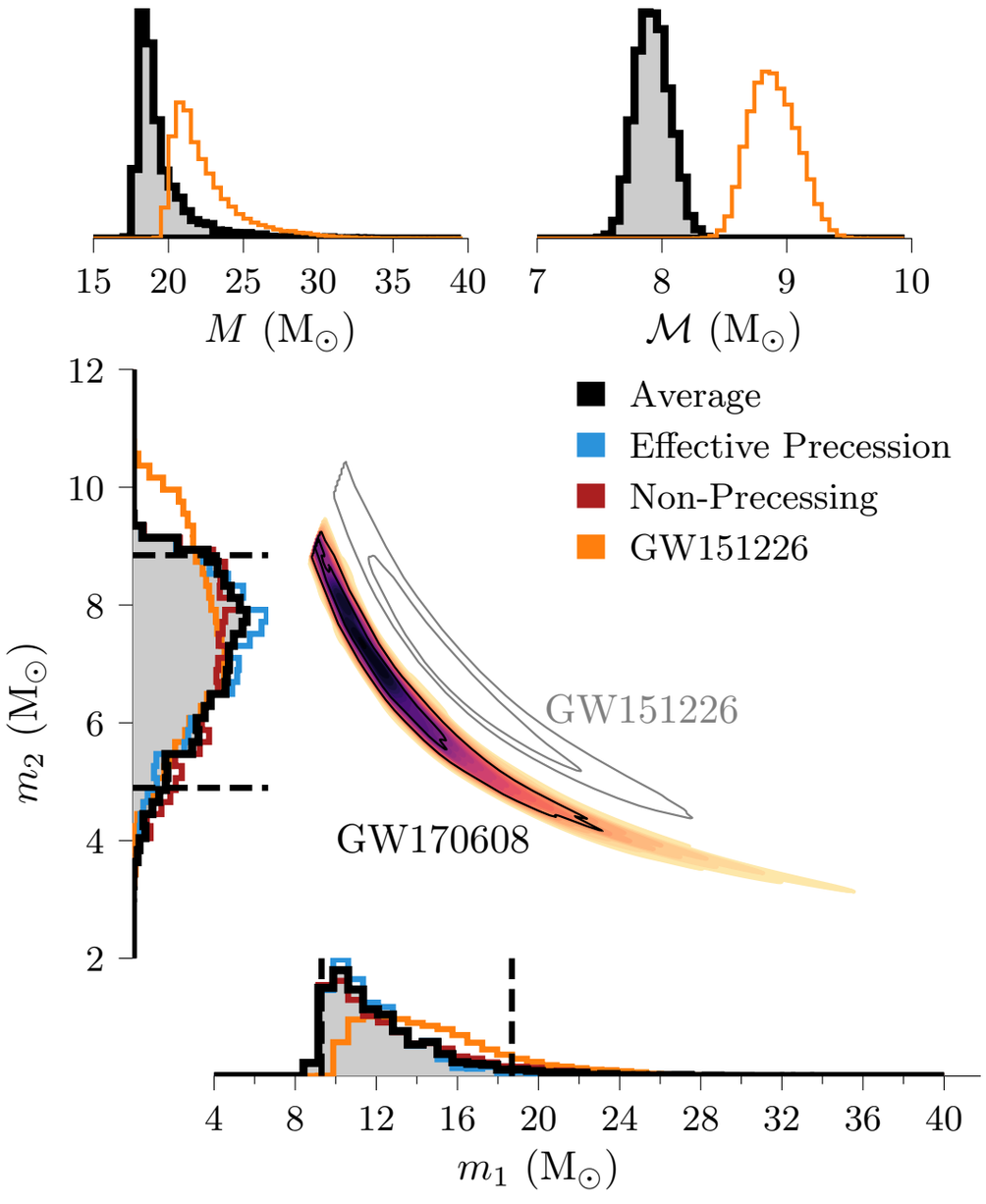

- **Chirp mass** is **best measured**. **Individual masses** can be **better measured** if **merger is observed**, because total mass is measured at merger.

Unveiling binary neutron star properties: masses

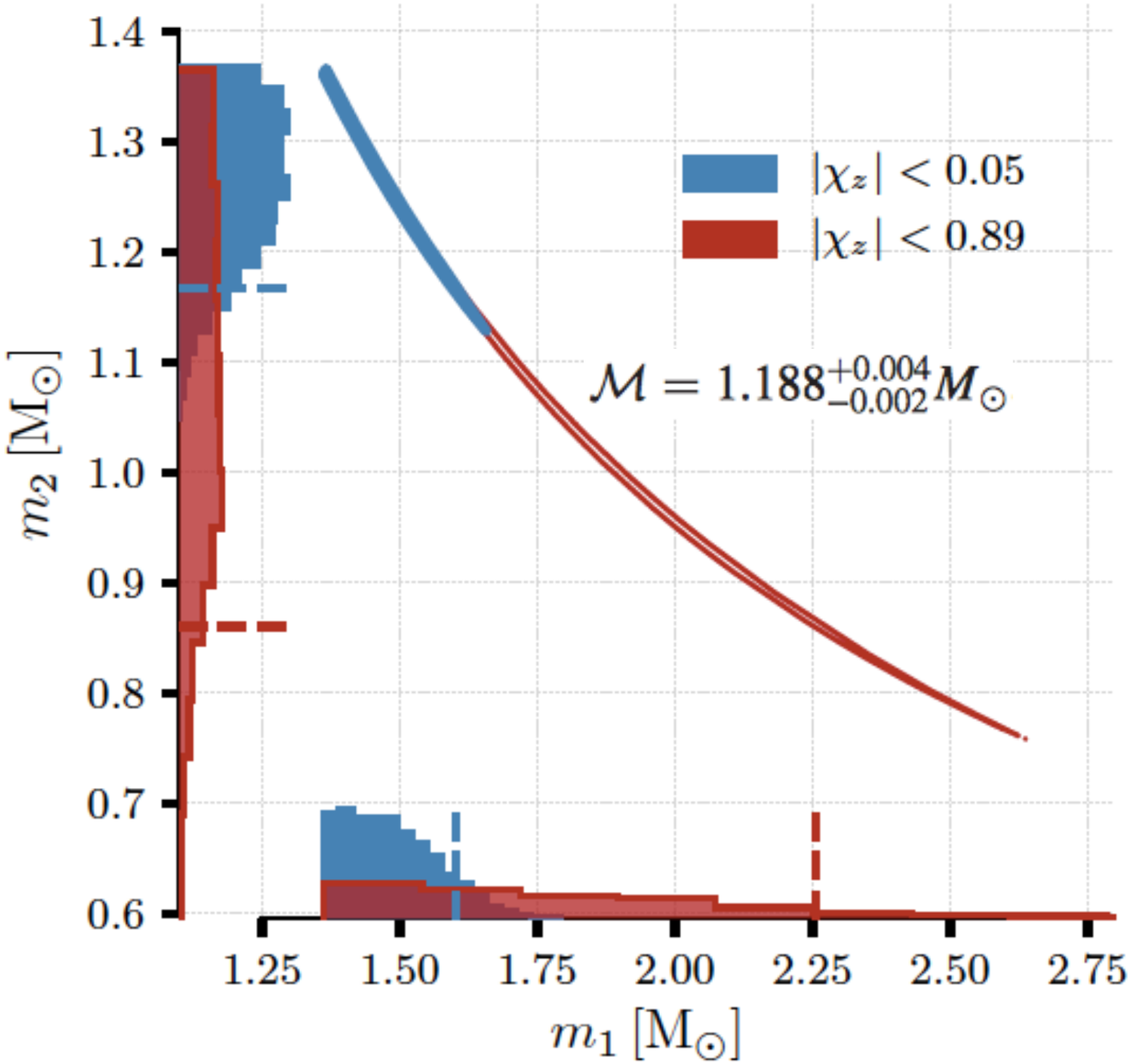

(Abbott et al. PRL 119 (2017) 161101)

- **Degeneracy** between masses and spins.
- **Fastest-spinning** neutron star has (dimensionless) **spin ~0.4.**
- Observation of **binary pulsars** in our galaxy indicate spins are **not larger than ~0.04**.

Unveiling binary black-hole properties: spins

(measurements @ 25Hz)

GW150914

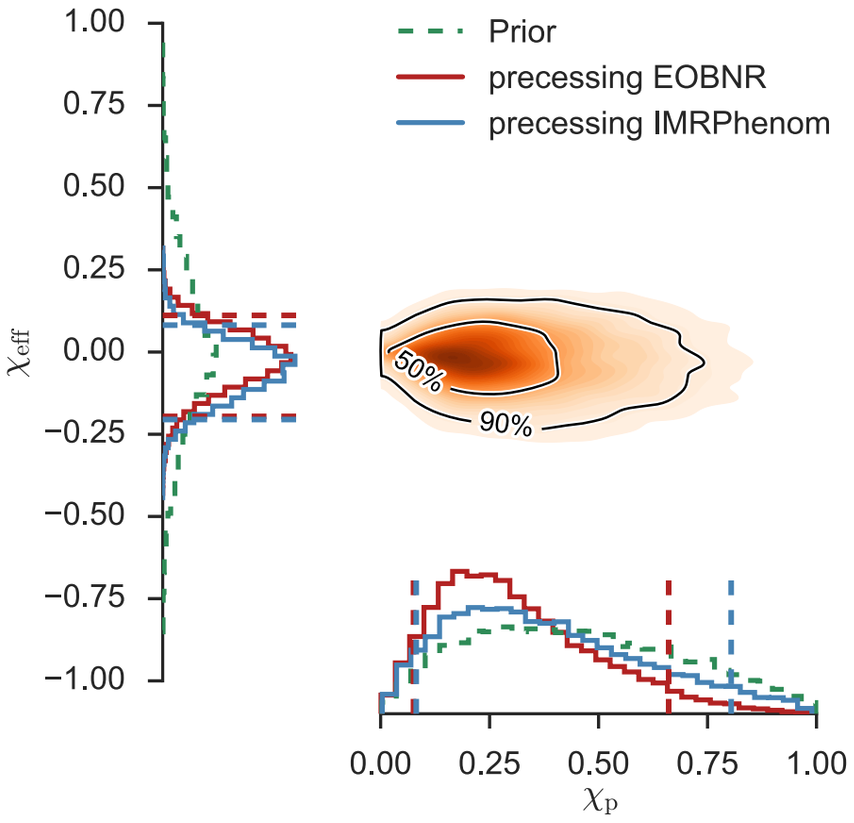

GW151226

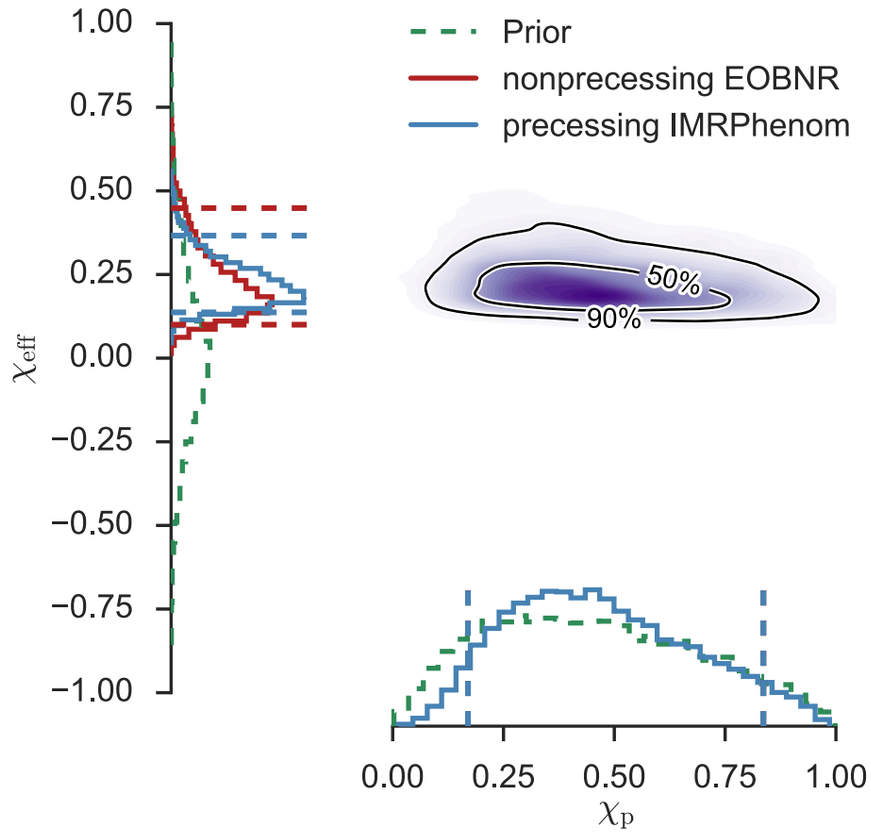

(*Abbott et al. PRX 6 (2016) 041014*)

(*Abbott et al. PRL 116 (2016) 241103*)

$$\chi_{\rm eff} = \frac{c}{GM}\left(\frac{\boldsymbol{S}_1}{m_1} + \frac{\boldsymbol{S}_2}{m_2}\right)\cdot\frac{\boldsymbol{L}}{|\mathbf{L}|}$$

(constant through 2PN order)

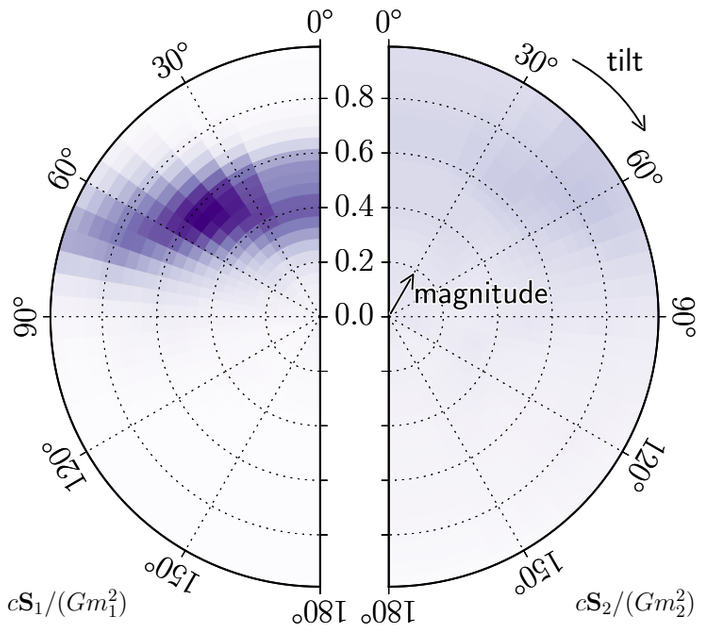

- BHs' **spins not maximal**, and for GW151226 **one BH's spin larger than 0.2** at 99% confidence.
- **Spins < 0.7. No information** about **precession**.

Unveiling binary black-hole properties: spins

(measurements @ 25Hz)

GW150914

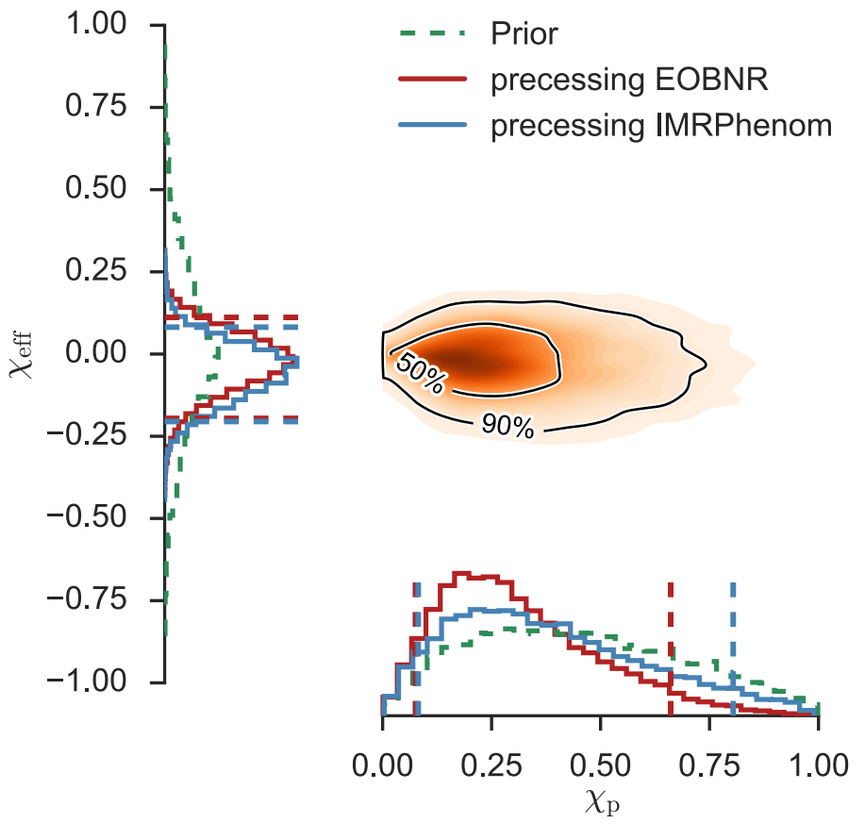

GW151226

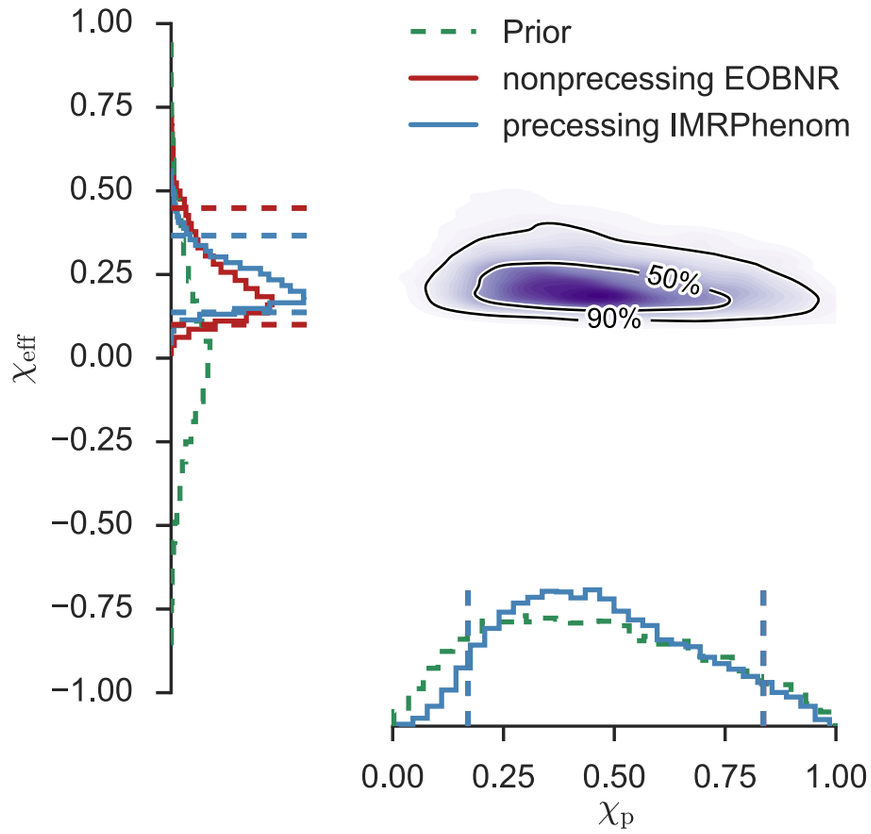

(*Abbott et al. PRX 6 (2016) 041014*)

(*Abbott et al. PRL 116 (2016) 241103*)

$$\chi_p = \frac{c}{B_1 G m_1^2} \max(B_1 S_{1\perp}, B_2 S_{2\perp})$$

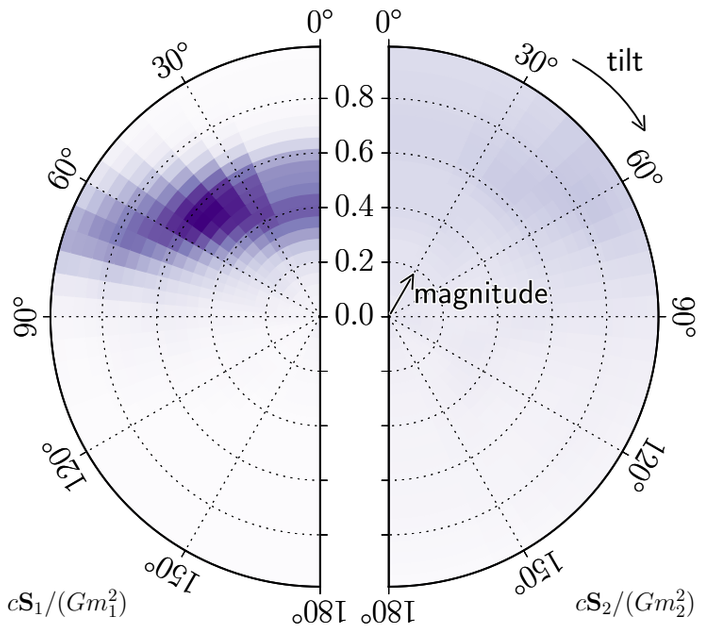

- BHs' **spins not maximal**, and for GW151226 **one BH's spin larger than 0.2** at 99% confidence.
- **Spins < 0.7. No information** about **precession**.

Unveiling binary black holes properties: spins

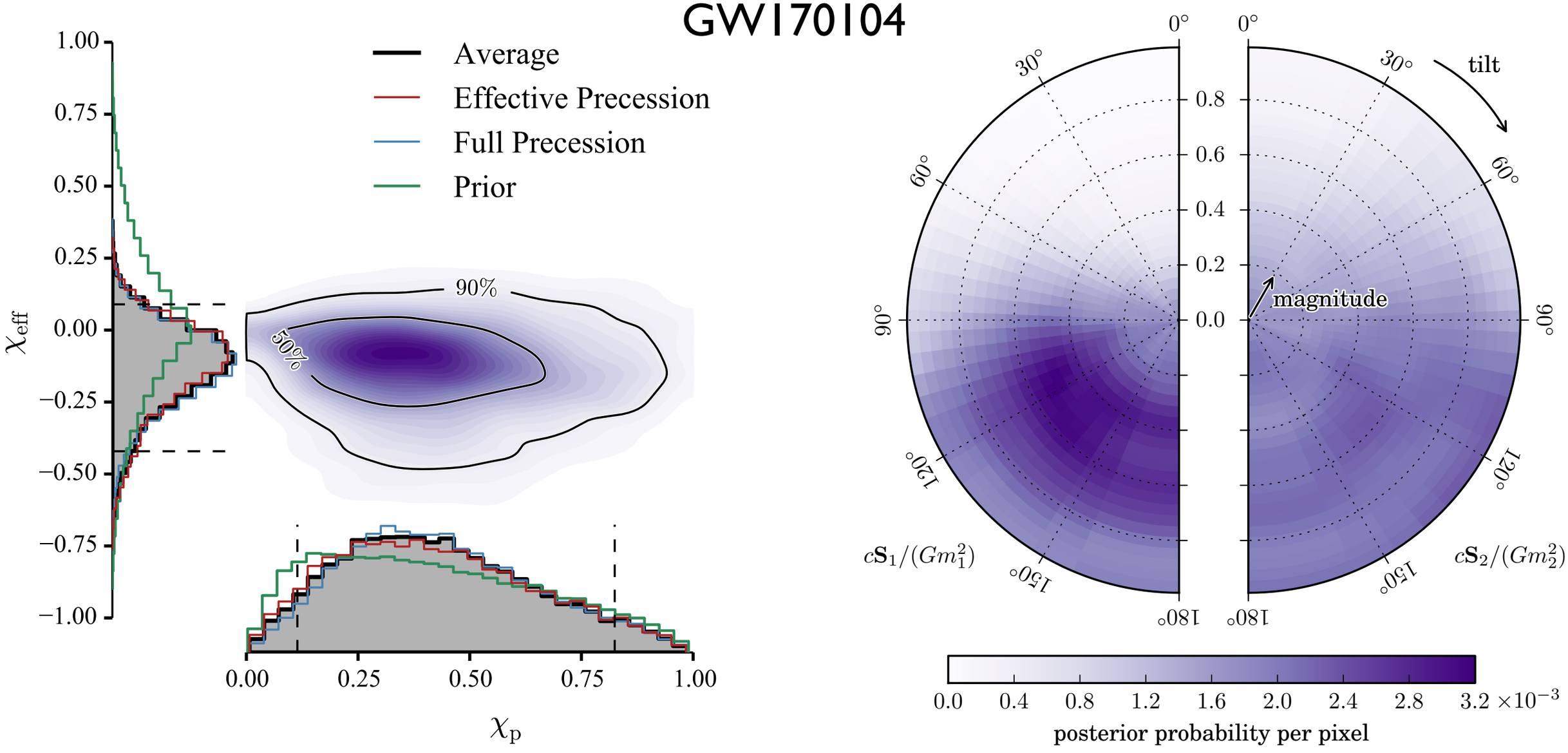

- **Probability that** $\chi_{\rm eff} < 0$ **is 82%** *(Abbott et al. PRL 118 (2017) 221101)*

- **Measurements disfavor** large total **spin positively aligned,** but **do not exclude zero spins.**

Binaries' distance and inclination

(Abbott et al. PRX 6 (2016) 041015)

GW150914

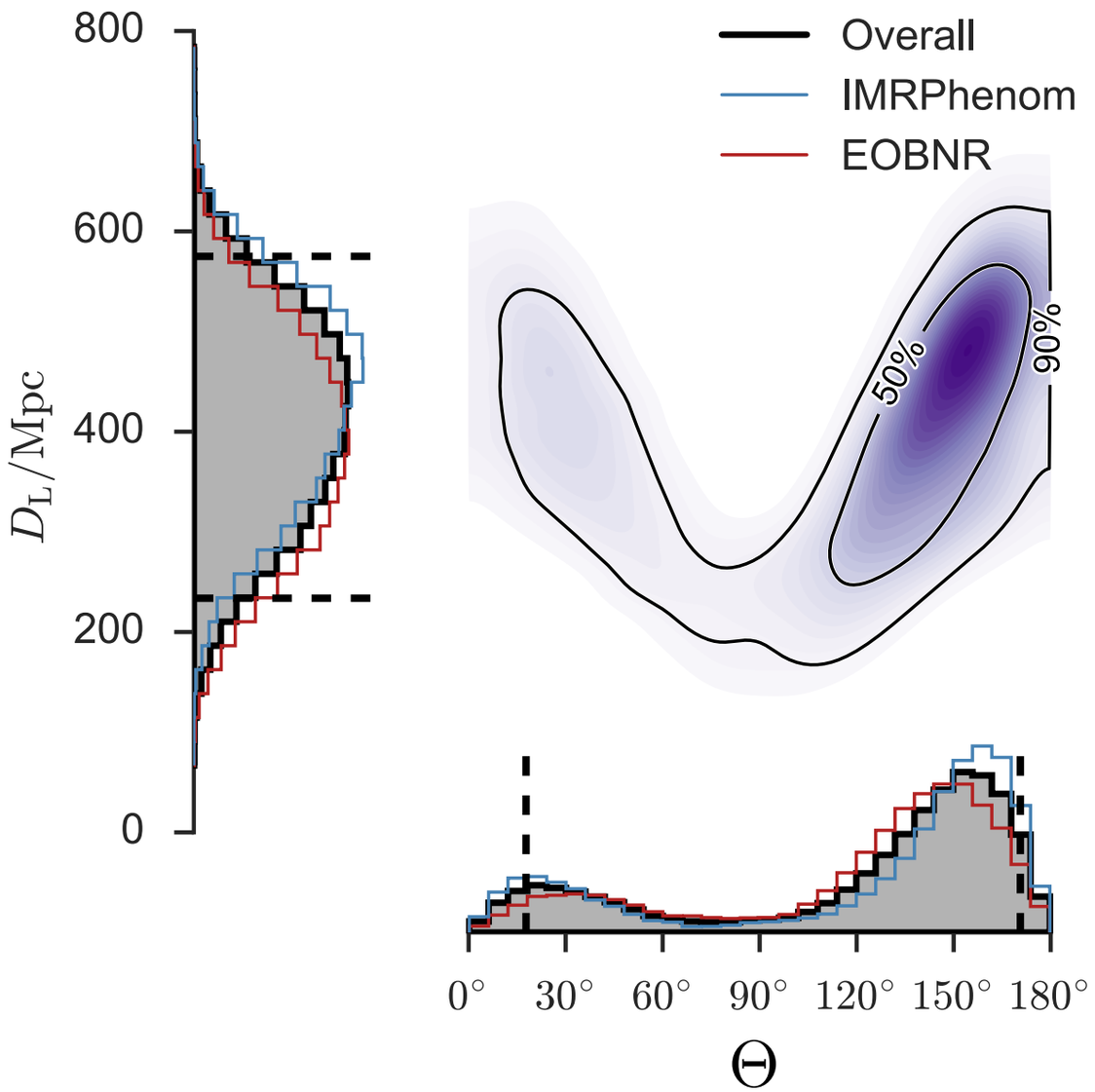

GW151226

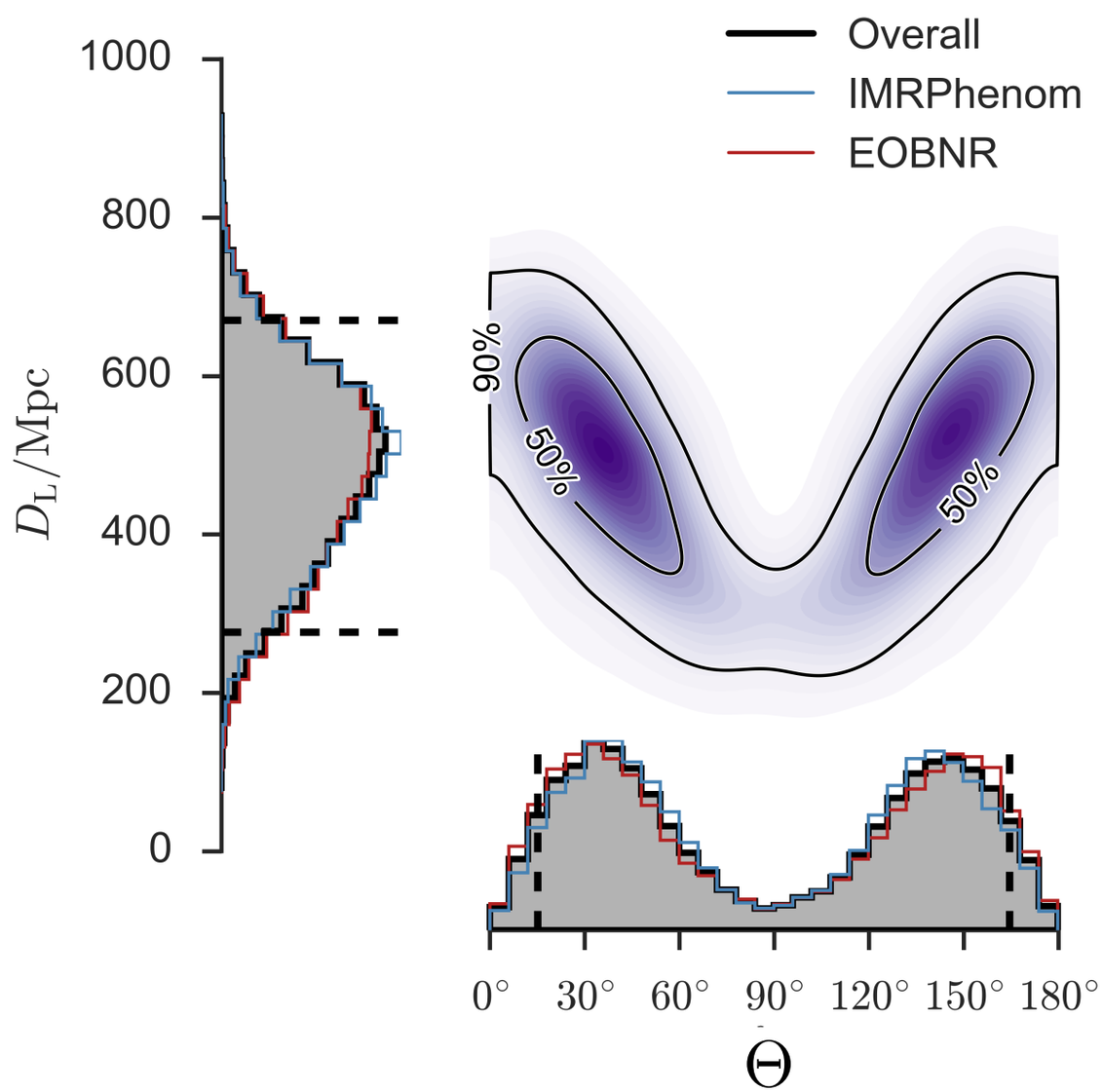

Effect of orientation of binary's orbital plane

spin nonprecessing binary

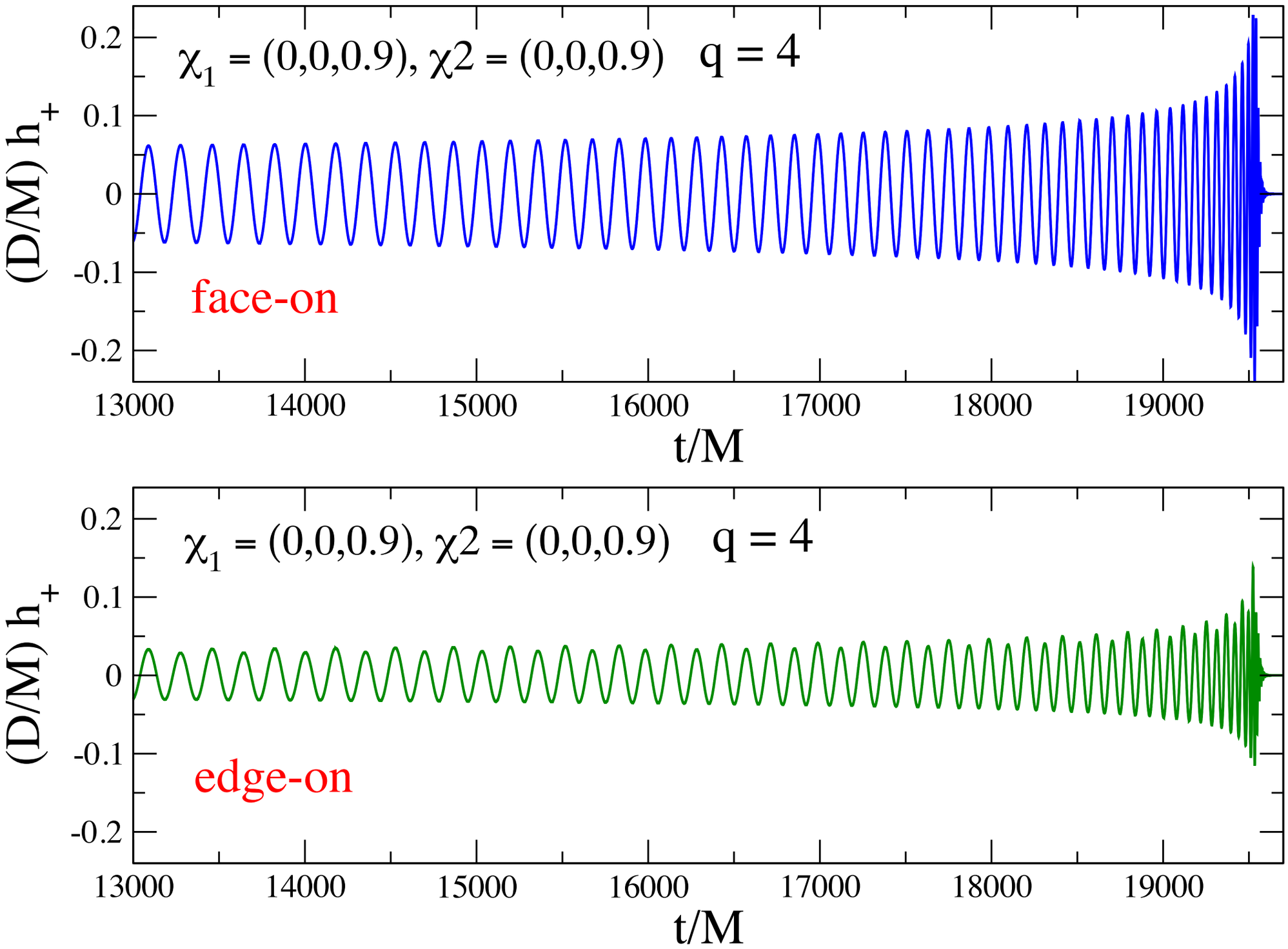

Effect of orientation of binary's orbital plane

spin precessing binary

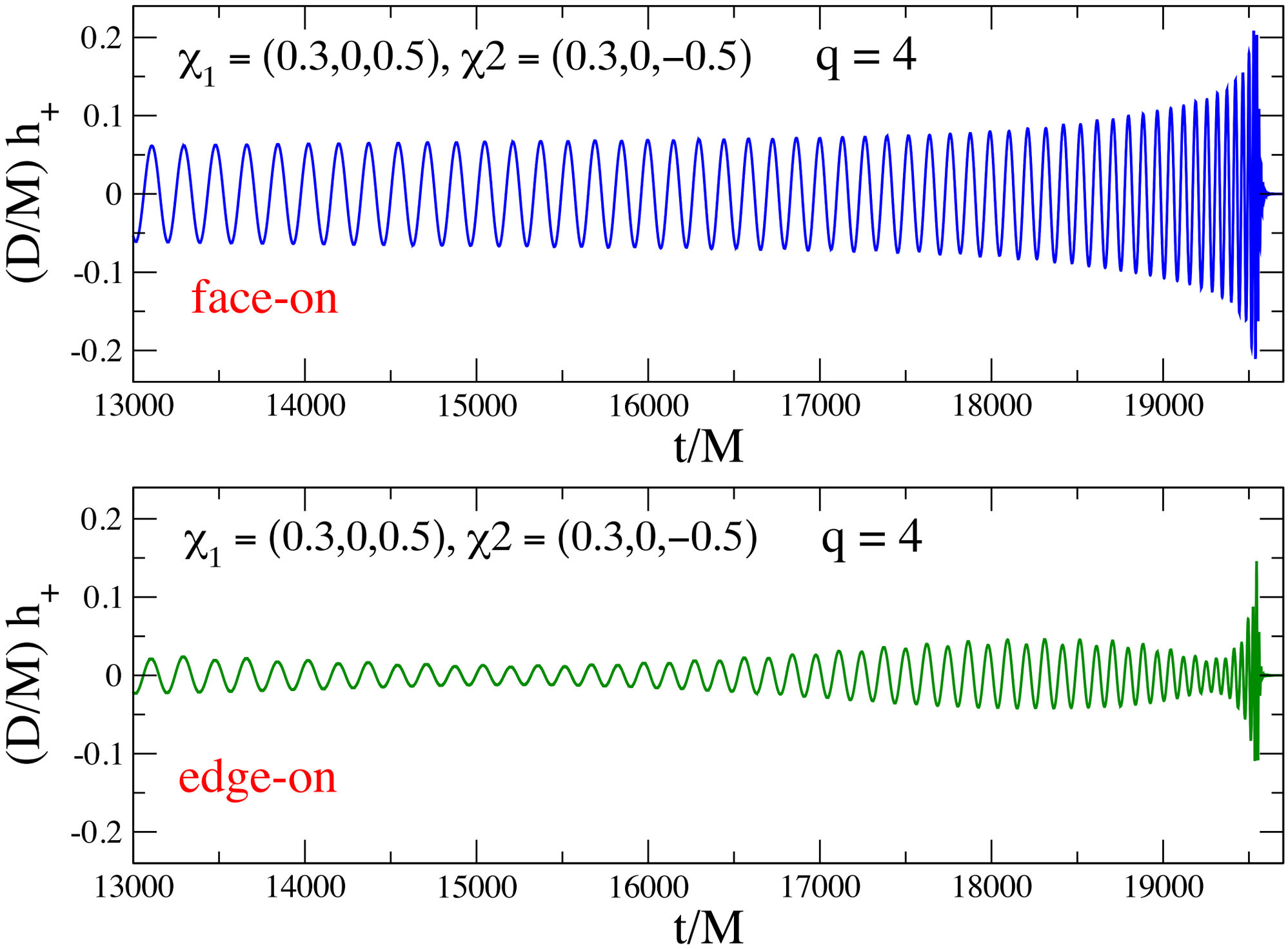

Importance of higher harmonics: varying mass ratio

$$h_+(t;\Theta,\varphi) - i\,h_\times(t;\Theta,\varphi) = \sum_{\ell=2}^{\infty}\sum_{m=-\ell}^{\ell} {}_{-2}Y_{\ell m}(\Theta,\varphi)\,h_{\ell m}(t)$$

(Cotesta, AB et al. 18)

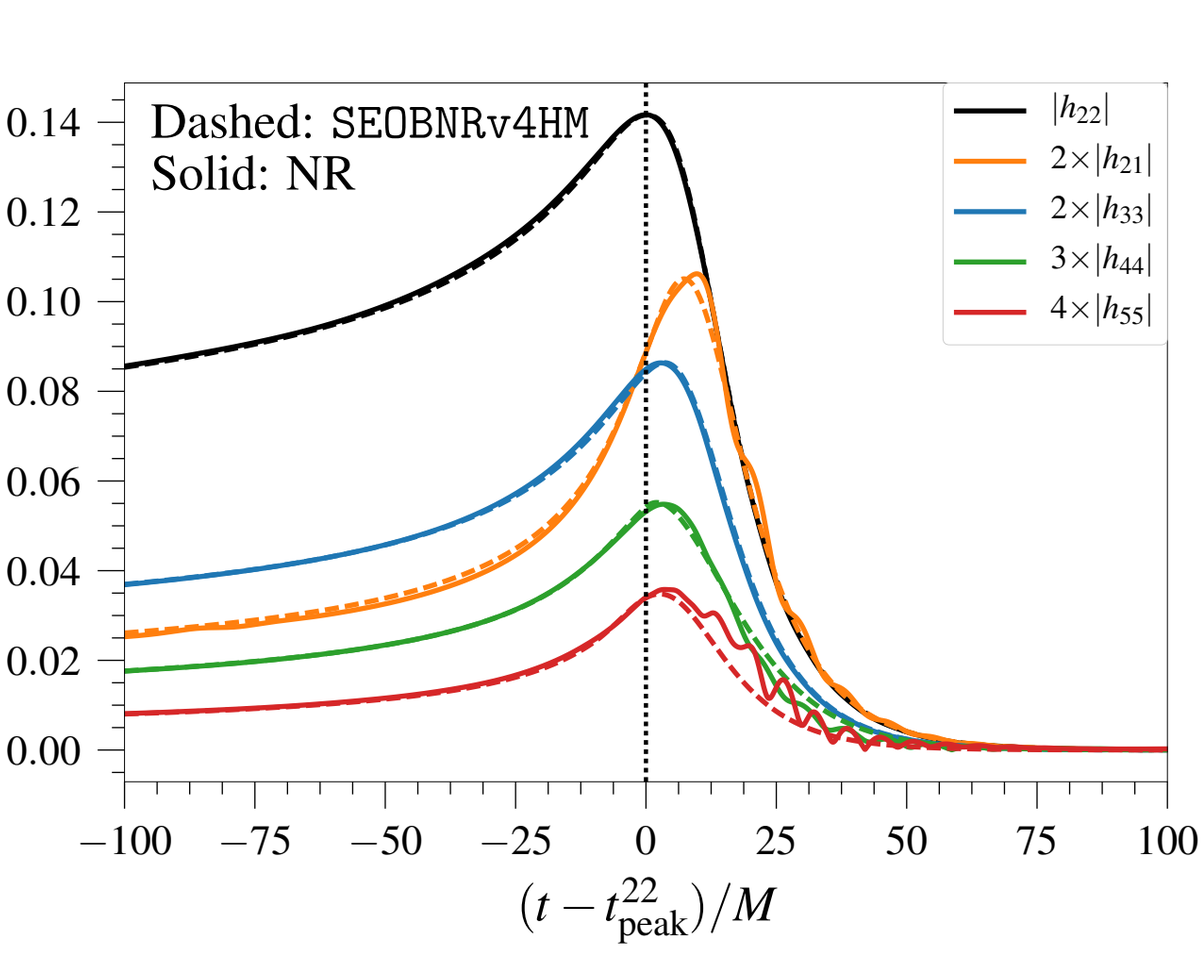

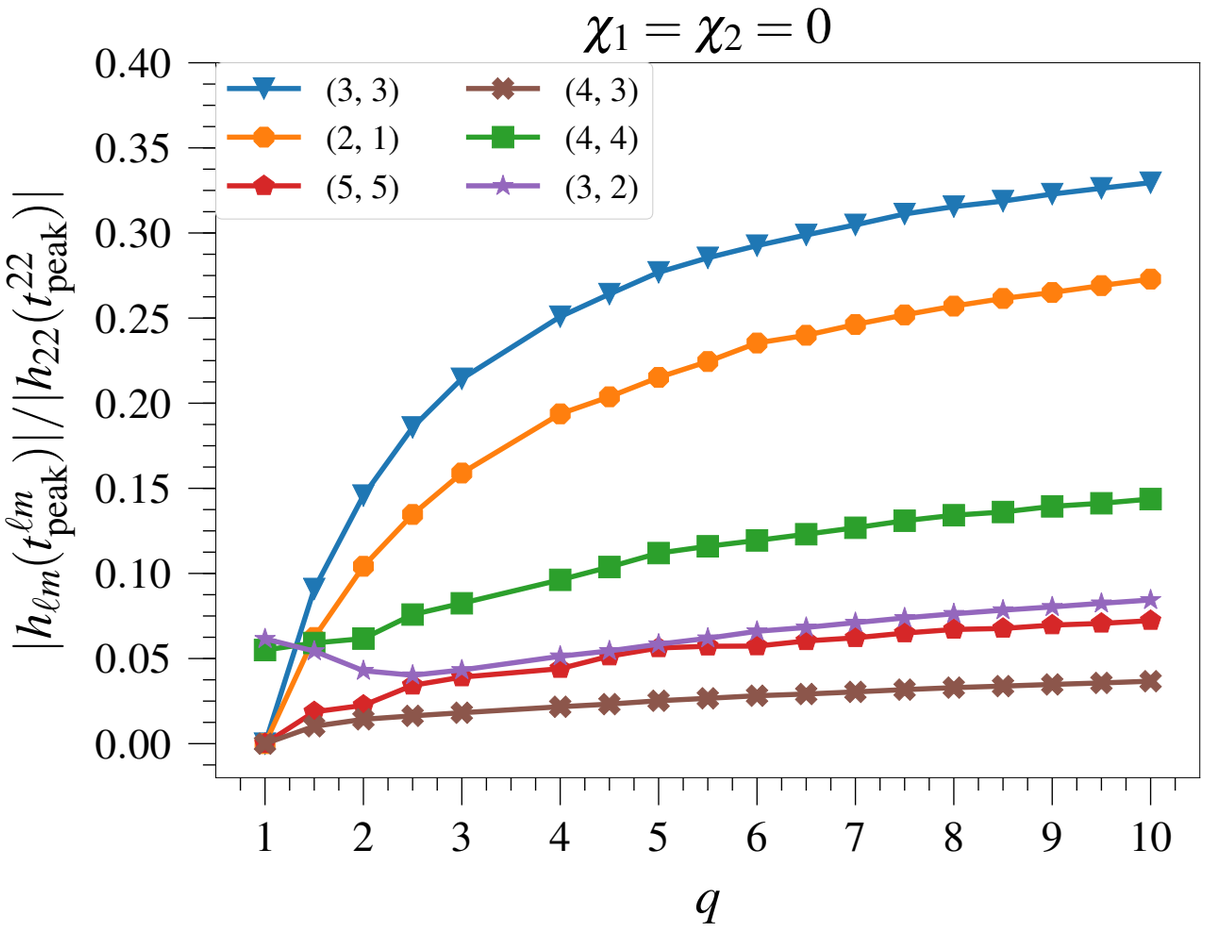

- Merger-ringdown EOBNR model **reproduces time & phase shifts between NR modes' at peak.**

Importance of higher harmonics also depends on geometric factor

$$h_+(t;\Theta,\varphi) - i\,h_\times(t;\Theta,\varphi) = \sum_{\ell=2}^{\infty}\sum_{m=-\ell}^{\ell} {}_{-2}Y_{\ell m}(\Theta,\varphi)\,h_{\ell m}(t)$$

geometric factor is important to determine **strength** of **higher harmonics**

(Cotesta, AB et al. 18)

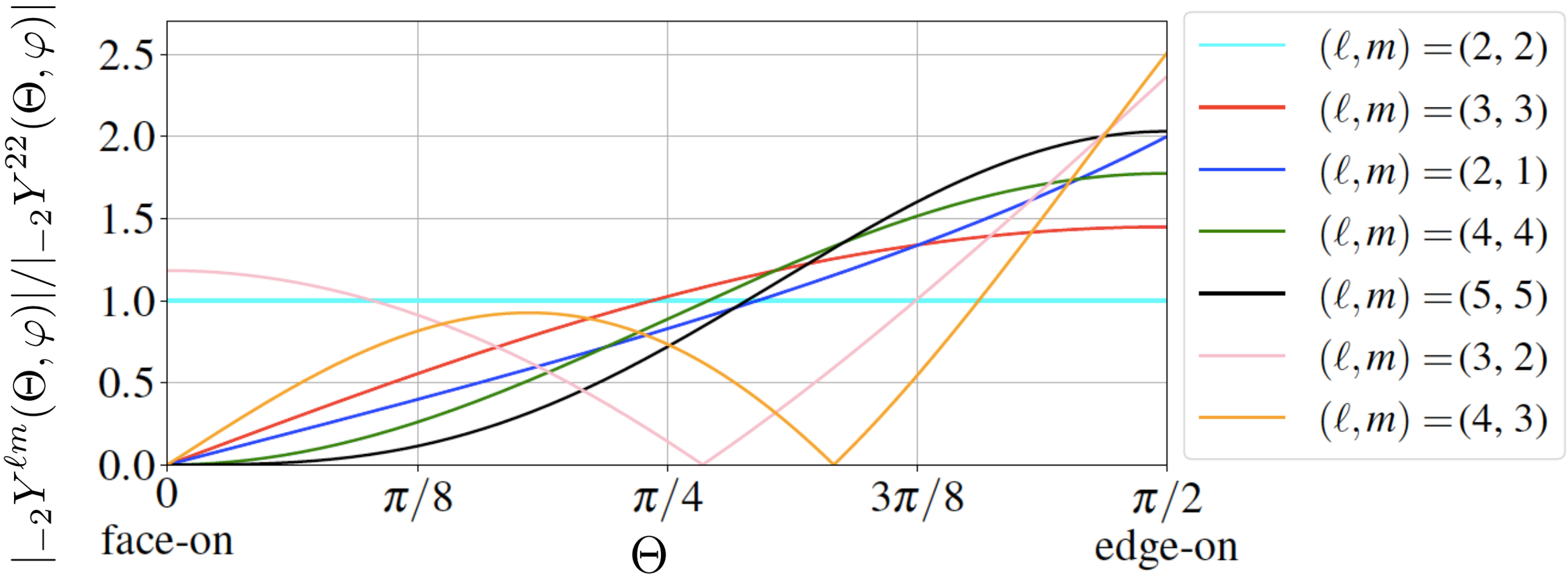

Accuracy of multipolar EOBNR model against NR

- **Non-precessing spin EOBNR** waveform model with **(2,1), (3,3), (4,4) & (5,5) modes.**

(Cotesta, AB et al. 18)

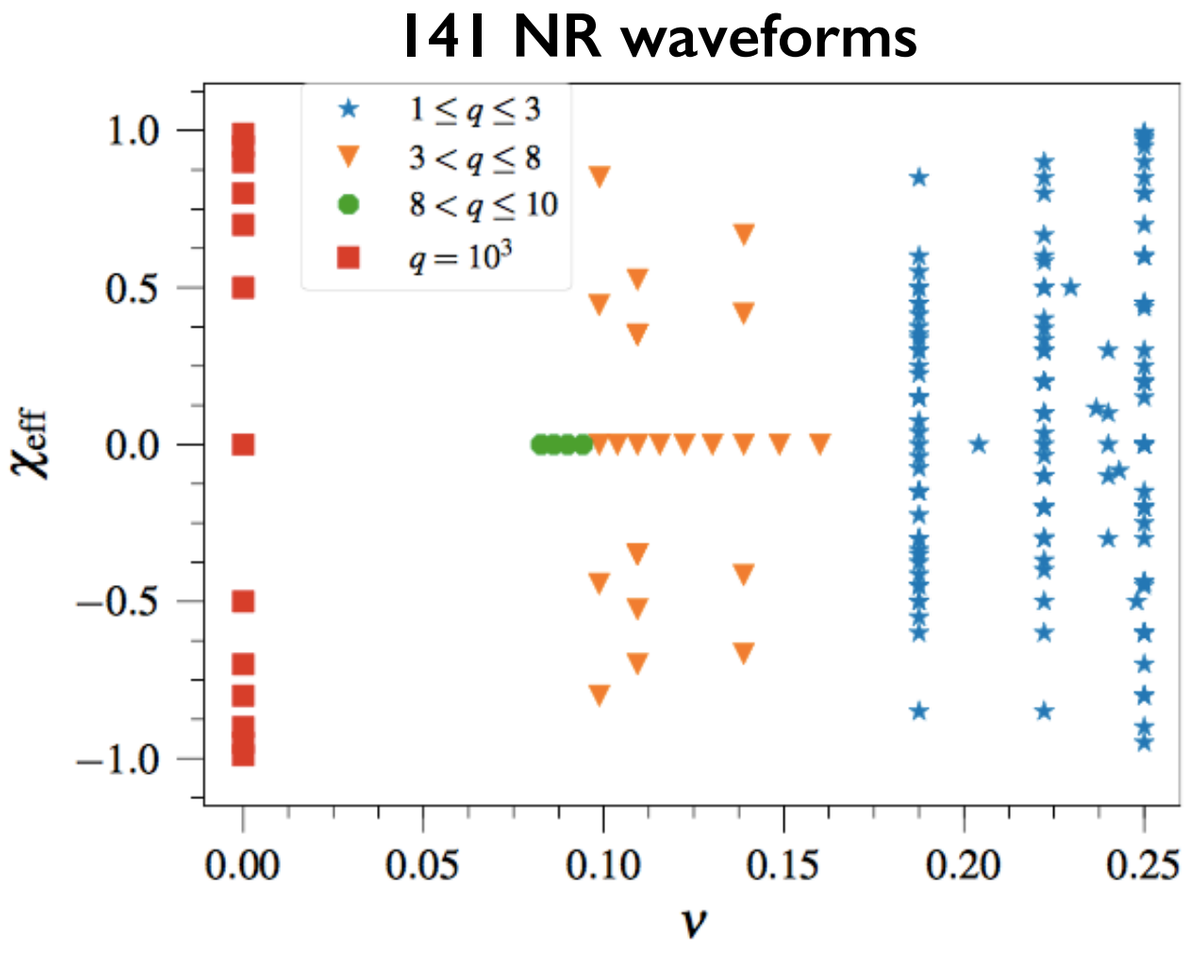

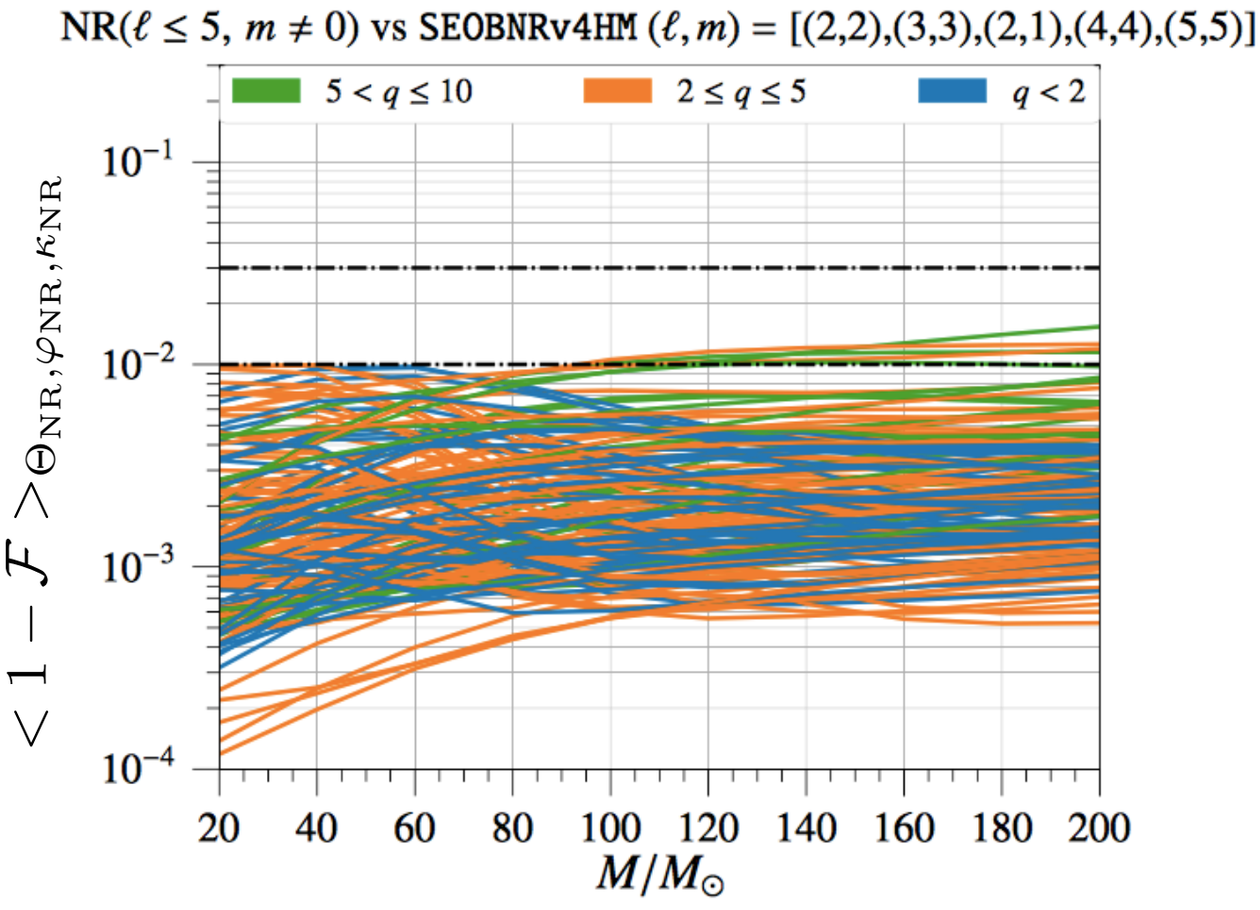

- **Extending analysis** to **other modes requires** producing **accurate NR waveforms** for those modes.

(for modeling see also Mehta et al. 17, London et al. 17; for searches see Capano, …, AB 16, Harry et al. 18)

Three-detector observation during O2: GW170814

(Abbott et al. PRL 119 (2017) 141101)

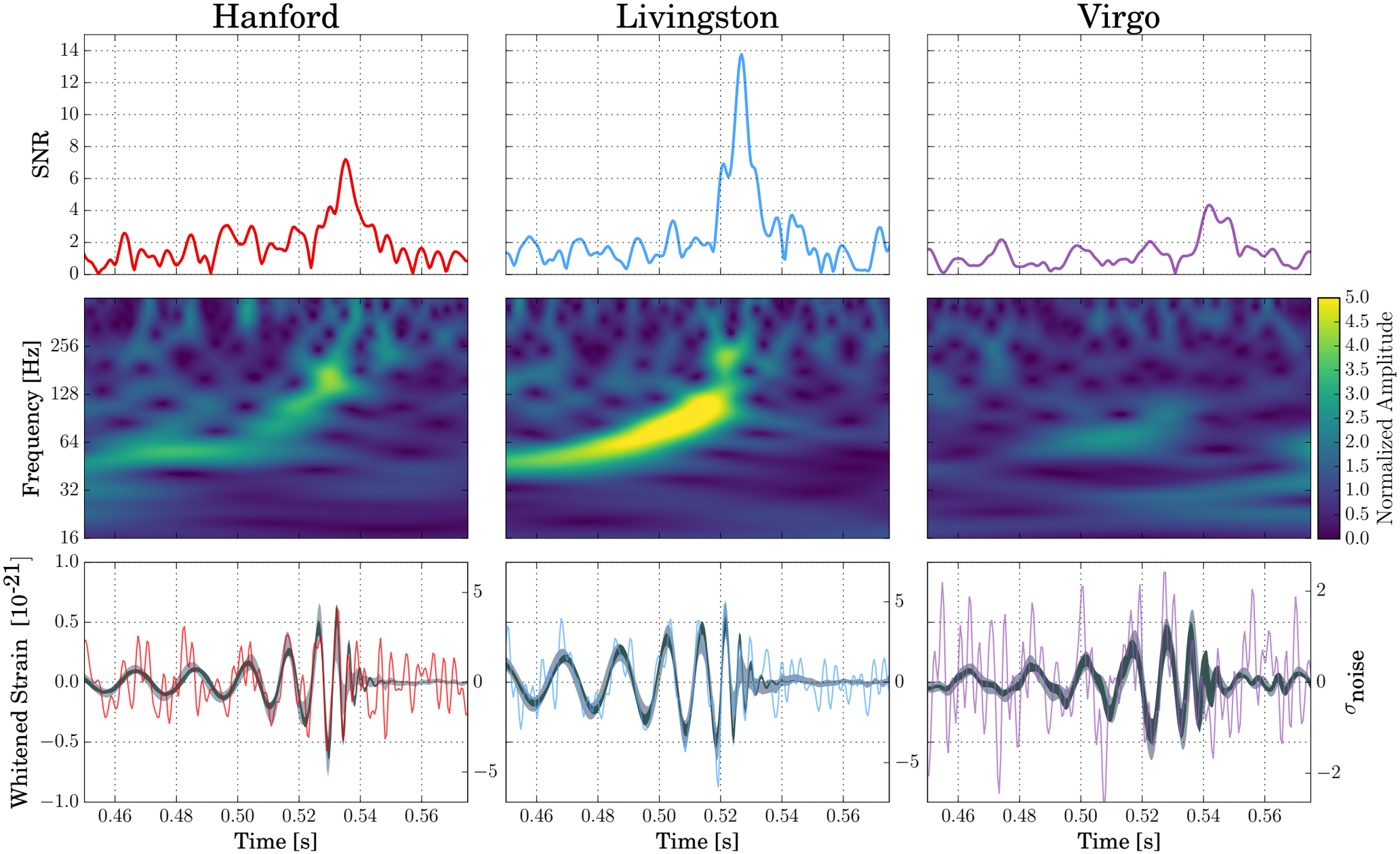

- **GW170814**: SNR=7.3 (Hanford), 13.7 (Livingston), 4.4 (Virgo)

Three-detector observation improves source sky-localization

(Abbott et al. PRL 119 (2017) 141101)

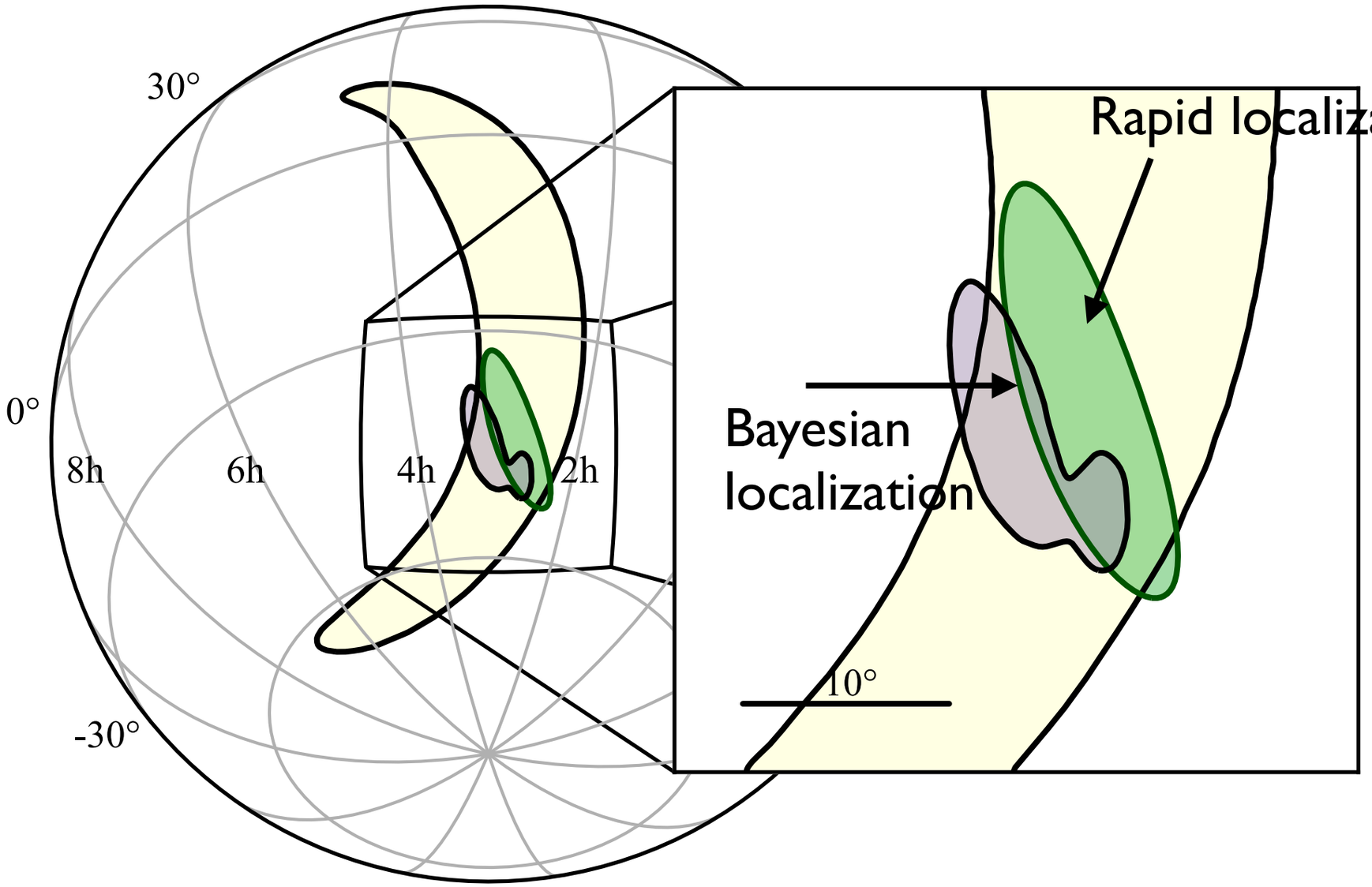

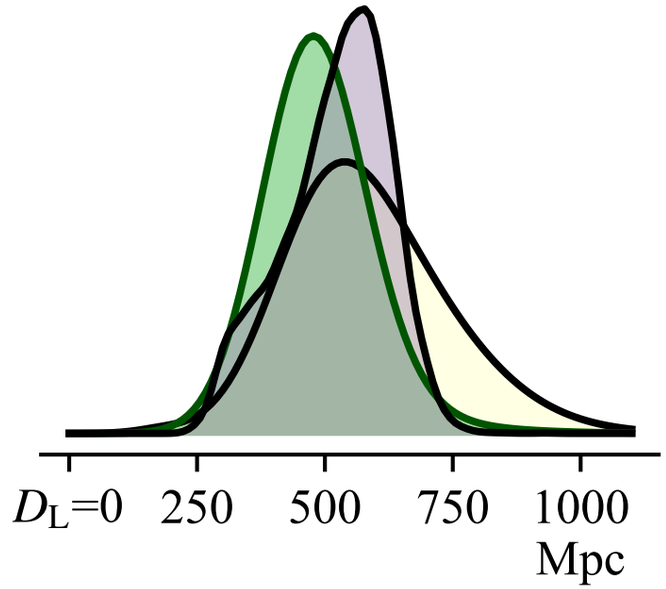

- GW **amplitude & phase information at different detectors** improve localization.

- **GW170814**: with Virgo, **sky-localization reduced** from 1160 to **60 square degrees** (90% credible regions). **Distance** measurement also **improved**.

Cosmography: Inference of Hubble constant with GW170817

- Compact-object **binaries are standard candles** (sirens). *(Schutz 1986)*
- **Standard candles** are **sources whose distance** from Earth can be **inferred from** their **luminosity**.

parameters

$$h(t) \propto \frac{1}{D} F(p_i) v^2(t; p_i) \cos[\phi_{\rm GW}(t; p_i)]$$

Hubble flow velocity

source's distance

$$v_H = H_0 D$$

Hubble constant

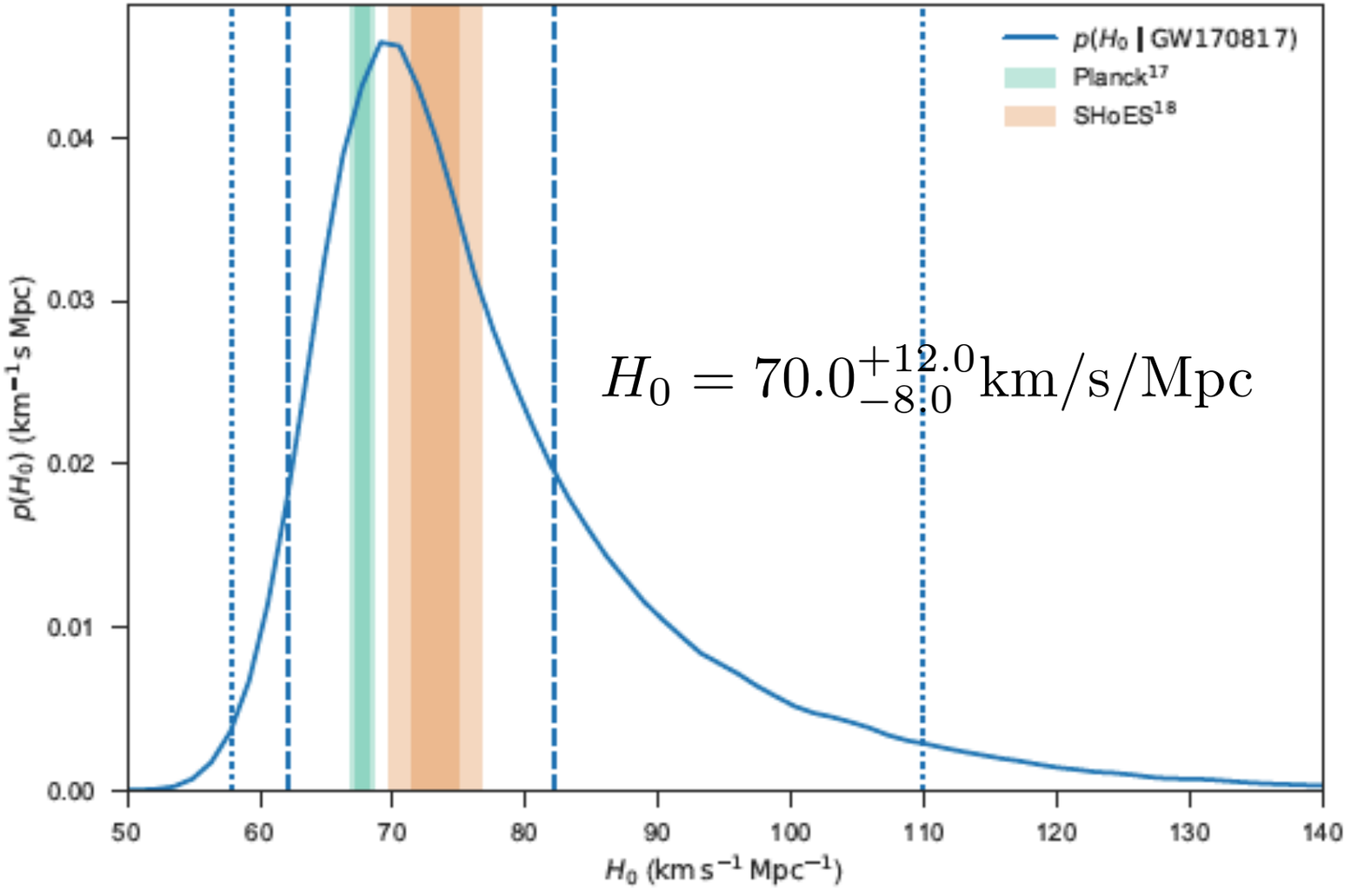

(Abbott et al. Nature (2017) 24471)

- We exploit identification of **host galaxy NGC4993 group** (through optical counterpart) to obtain Hubble flow velocity.

Sky localization and rapid EM follow up

- **28 square degrees**

03:05:23 August 18, 2017

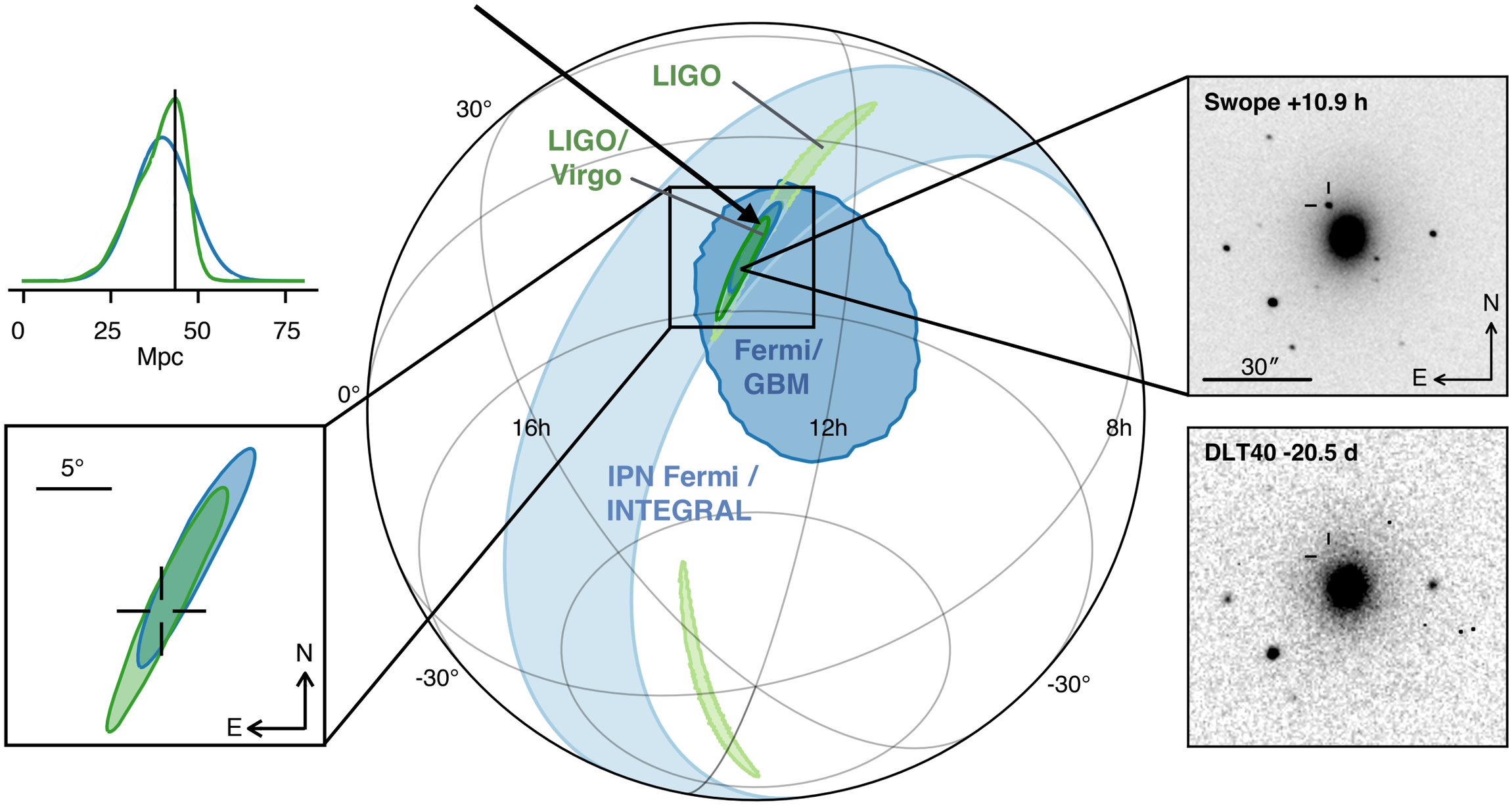

(Abbott et al. APJ 848 (2017) L12)

Hubble parameter correlates with binary's inclination

$$h(t) = \frac{2\mathcal{M}}{D}\,\mathcal{A}(\theta,\phi,\psi;\Theta)\,[\mathcal{M}\omega(t)]^{2/3}\,\cos(2\Phi(t)+2\Phi_0-\alpha)$$

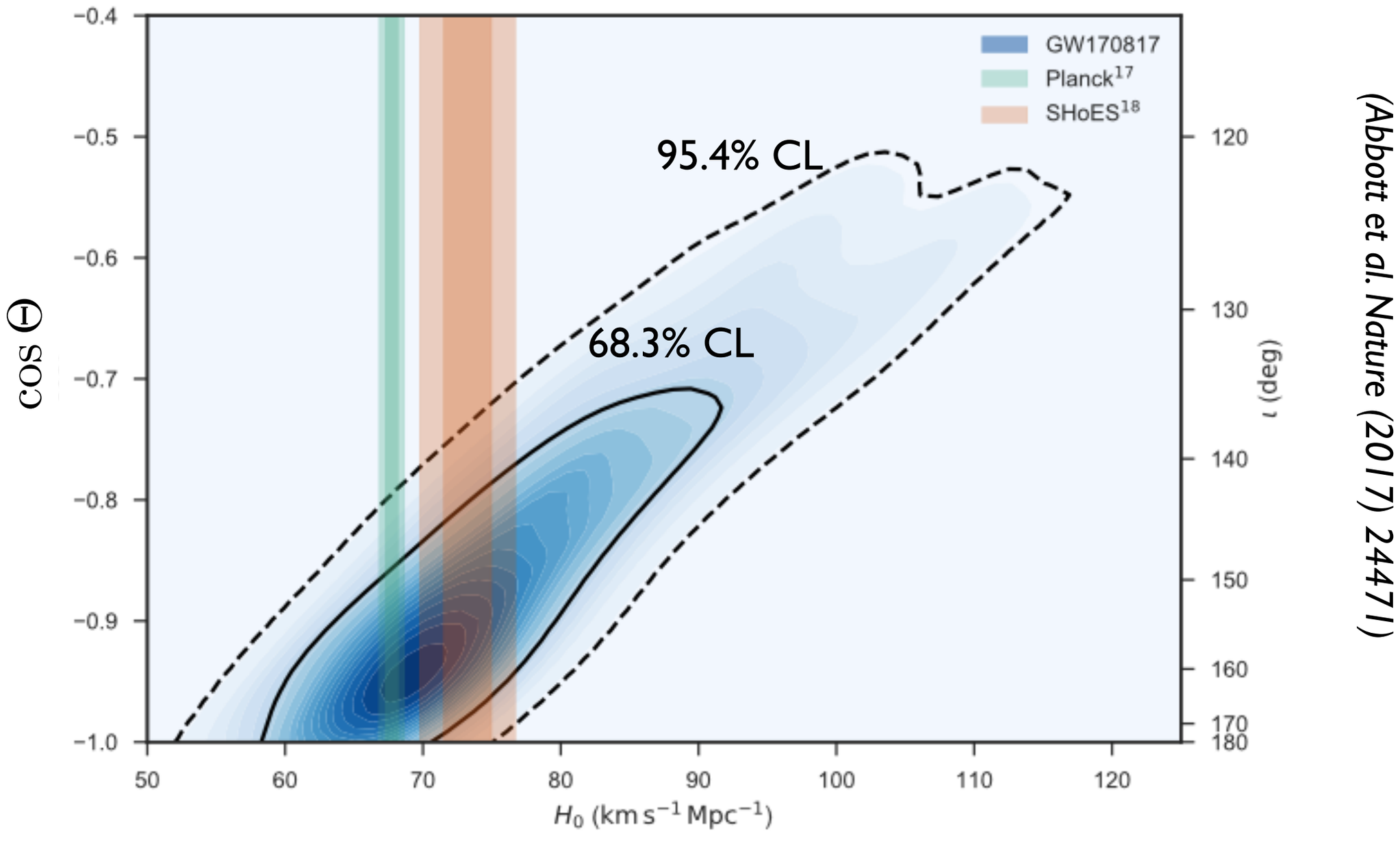

(Abbott et al. Nature (2017) 24471)

Constraints on binary's inclination angle using Planck/SHoES